https://doi.org/10.5194/egusphere-2026-6347
Preprint. Discussion started: 5 November 2026
© Author(s) 2026. CC BY 4.0 License.

Spatial Patterns of Temperature and Precipitation Extremes Across Spain Under Climate Change: A Comparison of Bayesian Approaches

Soledad Collazo[1], David Barriopedro[2], Ricardo García-Herrera[1,2], José Agustín García[3], Santiago Beguería[4], Juan Emmanuel Johnson[5], Sergio M. Vicente-Serrano[6]

[1]Departamento de Física de la Tierra y Astrofísica, Facultad de Ciencias Físicas, Universidad Complutense de Madrid, Madrid, 28040, Spain
[2]Instituto de Geociencias (IGEO), Consejo Superior de Investigaciones Científicas– Universidad Complutense de Madrid, Madrid, Spain
[3]Departamento de Física, Universidad de Extremadura, Badajoz, Spain
[4]Estación Experimental de Aula Dei-Consejo Superior de Investigaciones Científicas (EEAD-CSIC), Zaragoza, Spain
[5]International Methane Emissions Observatory, Mitigation Branch–Climate Change Division, United Nations Environment Programme, Paris, France
[6]Instituto Pirenaico de Ecología, Consejo Superior de Investigaciones Científicas (IPE- CSIC), Zaragoza, Spain

Correspondence to: Soledad Collazo (scollazo@ucm.es)

Abstract. Characterizing the spatio-temporal behavior of extreme events remains statistically challenging since they are inherently rare. This study quantifies the response of temperature and precipitation extremes across Spain to global warming using a hierarchical Bayesian framework that jointly estimates spatially varying model parameters and their uncertainty across a dense network of weather stations over 1981–2022. Summer daily temperature extremes (TXx) increased markedly with global warming, especially in central and western Spain, whereas autumn daily precipitation extremes (Rx1day) showed no detectable response. Therefore, TXx required a non-stationary model, whereas Rx1day could be fairly described assuming stationarity. Concerning spatial dependence, two strategies were compared: a two-step approach combining local model fitting with universal kriging, and a fully spatial Bayesian model, with the latter providing better-calibrated predictions and a more coherent quantification of uncertainty, especially for the non-stationary TXx model. Temperature and precipitation extremes also showed contrasting geographic patterns: TXx magnitude decreased with elevation and coastal proximity, though its interannual variability peaked along coasts. Conversely, both the mean intensity and variability of Rx1day increased with elevation and closeness to the sea. These contrasting behaviors have direct implications for future risk. Under a scenario of 2.5 °C of global warming, 100-year return levels for summer TXx are projected to approach 50 °C across southwestern Spain, whereas the selected stationary model estimates autumn Rx1day return levels exceeding 200 mm along the Mediterranean coast. Climate adaptation planning must therefore address both a rapidly intensifying heat signal and a precipitation hazard that remains severe.

https://doi.org/10.5194/egusphere-2026-6347
Preprint. Discussion started: 5 November 2026
© Author(s) 2026. CC BY 4.0 License.

1 Introduction

In recent decades, extreme weather events, like heatwaves and intense precipitation, have become more frequent and severe over many land areas (IPCC AR6, 2023). This has raised concerns about their potential societal, economic, and environmental impacts. Spain is an example of these changes. Since the 1960s, the mean surface air temperature has risen by approximately 0.3 °C per decade (Corell et al., 2026). This increase is predominantly driven by a rise in warm extremes rather than a comparable decrease in cold extremes (Castillo-Mateo et al., 2023). Heatwaves have also become more frequent, persistent, and intense than cold spells across mainland Spain since the early 1980s (Serrano-Notivoli et al., 2022; Vicente-Serrano et al., 2017). In contrast, there has been little change in precipitation since 1871, with pronounced multi-decadal and interannual variability primarily driven by atmospheric circulation rather than a discernible long-term trend (Vicente-Serrano et al., 2025a). Similarly, no significant changes in the frequency or intensity of extreme precipitation events have been observed since 1961 (Vicente-Serrano et al., 2025b). Nevertheless, extreme rainfall continues to have devastating consequences, as evidenced by the floods in eastern Spain in 2024, which resulted in over 200 fatalities and billions of euros in economic losses (Barriopedro et al., 2025; Calvo-Sancho et al., 2026).

In this context, developing robust statistical frameworks that characterize the spatiotemporal evolution of extreme events across Spain becomes essential. Extreme Value Theory (EVT) provides a well-known approach for fitting the tail behavior of probability distributions and, consequently, the occurrence of extreme events (Coles, 2001). There are two main statistical paradigms, frequentist and Bayesian, which offer different tools for estimating EVT model parameters, each with distinct advantages and limitations. Frequentist approaches commonly employ maximum likelihood estimation (MLE), in which parameters are regarded as fixed constants to be estimated (Yılmaz et al., 2021). In contrast, Bayesian methods treat parameters as random variables and combine prior distributions with the data to obtain a posterior distribution, which is typically sampled using Markov chain Monte Carlo (MCMC) algorithms (Bousquet, 2021). Simulation studies and empirical applications to flood, wind, and rainfall extremes (e.g., Ahmad et al., 2022; Diriba and Debusho, 2020; García et al., 2024) have shown that Bayesian estimators can outperform frequentist ones in terms of bias, mean square error, and precision, particularly when prior knowledge is available or sample sizes are limited. Bayesian approaches also yield credible intervals (CIs) that provide a more realistic representation of uncertainty, although their sensitivity to prior selection and higher computational demands can be challenging.

Under climate change, a central challenge is to assess its influence on the behavior of extreme events. This is often implemented by assuming that one or more parameters of the distribution vary smoothly with time or global mean temperature (Philip et al., 2020), leading to the formulation of a non-stationary EVT, a framework that models how the probability or magnitude of extremes evolves with global warming. Depending on data availability and study objectives, extreme value estimation can be performed using models that focus solely on time series analysis or those that jointly account for spatial and temporal

https://doi.org/10.5194/egusphere-2026-6347
Preprint. Discussion started: 5 November 2026
© Author(s) 2026. CC BY 4.0 License.

variability. Temporal EVT models analyze time series at individual sites and are efficient for local assessments or short-term prediction (Castro-Camilo and Huser, 2020). However, they may overlook spatial dependencies that are often critical in climate and hydrological extremes (Davison et al., 2012; Huser and Wadsworth, 2022). Accounting for spatial information is particularly valuable because extreme events are rare and reliable estimation of their probability distributions requires long observational records, which are often limited by missing observations, changes in instrumentation, or insufficient spatial coverage. In this context, information from neighboring stations and geographic covariates can improve model performance and reduce estimation uncertainty (Cooley et al., 2007; Zhang et al., 2022). Spatio-temporal EVT models integrate both dimensions, allowing for the joint characterization of extremes across multiple locations and through time. These models frequently use covariates such as meteorological variables, topographic information, geographical coordinates, or vegetation indices to improve parameter estimation, facilitate physical interpretation, and generate spatially coherent return-level maps (Bacro et al., 2020; Cooley et al., 2007; Davison et al., 2012; García et al., 2018, 2024; Zhang et al., 2022). Although computationally demanding, spatio-temporal approaches are increasingly applied in climate attribution studies (e.g. Zanger et al., 2024), because they enable coherent regional inference and more rigorous uncertainty quantification.

Previous studies applied hierarchical Bayesian spatio-temporal models to analyze extreme summer temperatures and rainfall across Spain. For temperature, non-stationary models that incorporate global mean temperature as a covariate have been shown to provide a superior fit when compared to their stationary counterparts, indicating disproportioned increases in return levels with global warming (García et al., 2021, 2023, 2024). For extreme rainfall, hierarchical Bayesian models have substantially reduced parameter uncertainty compared to site-specific analyses, and non-stationary formulations driven by climate indices such as the North Atlantic Oscillation have improved the representation of temporal variability in extreme precipitation (García et al., 2018; Urrea Méndez and del Jesus, 2023). However, previous studies have not comprehensively evaluated extremes of both variables within a unified Bayesian spatio-temporal framework that compares alternative methodological choices.

The objective of this study is to develop and evaluate a Bayesian spatio-temporal framework for modelling daily temperature and precipitation extremes separately and their associated uncertainty across Spain during the period 1981–2022. The two types of extremes are modelled independently, allowing their spatial and temporal patterns to be characterized and contrasted. To this end, two alternative strategies for incorporating spatial dependence and predicting extremes at unobserved locations are implemented and assessed. In addition, the role of climate change is investigated by comparing stationary and non-stationary formulations of the extreme value models, thereby assessing whether its inclusion improves the description and prediction of climate extremes.

2 Data

Daily observations of maximum temperature and precipitation were obtained from mainland Spanish weather stations for the period 1981–2022, provided by the Spanish Meteorological Agency (AEMET). Gaps were addressed through a reconstruction procedure based on quantile mapping (Beguería et al., 2025). Homogenization was then applied to the completed station

https://doi.org/10.5194/egusphere-2026-6347
Preprint. Discussion started: 5 November 2026
© Author(s) 2026. CC BY 4.0 License.

records under the PTI-Clima project protocol to address possible shifts caused by instrumentation, relocations or observational practices (PTI-Clima, 2026).

To sample extreme values from the observed series we used the block maxima method, which extracts the highest observation within a fixed temporal block (Beguería et al., 2025). Seasonal block maxima for summer (JJA) maximum temperatures (TXx) and autumn (SON) daily precipitation totals (Rx1day) were selected as the extreme indices of interest. These seasons were chosen because they tend to capture the most intense extremes of the year (Barriopedro et al., 2025; Gonzalez-Hidalgo et al., 2025; Serrano-Notivoli et al., 2022). To limit the influence of gap-filling on model estimates, we computed the percentage of missing raw daily values within each season of each year (i.e., each individual summer for TX or each individual autumn for Rx1day), and excluded stations for which more than three of these seasonal periods had 10% or more missing values. After applying this criterion, 207 stations were retained for temperature and 341 for precipitation, providing large but spatially uneven coverage of peninsular Spain. The remaining stations that did not meet this criterion (1532 for temperature and 2108 for precipitation) were not used to fit the model but were retained for independent evaluation, enabling an out-of-sample assessment of model performance across a broad network of stations.

Global warming is represented by the annual global-mean temperature anomaly relative to 1850–1900 from HadCRUT5 (Met Office, 2024; Morice et al., 2021). To retain the slowly varying of this signal, the series was smoothed with a LOESS filter (Cleveland et al., 1992), which removes year-to-year fluctuations. The smoothed series is denoted Global Mean Surface Temperature (GMST). An earlier application of this data-processing strategy is described by Collazo et al. (2025).

3 Methodology

3.1 Generalized Extreme Value Distribution

According to EVT, block maxima are asymptotically distributed following a Generalized Extreme Value Distribution (GEVD), which is widely used in climatology, hydrology, and environmental sciences to characterize extreme events (e.g., Stott et al., 2016). The distribution is defined by three parameters (Eq. 1): a location parameter (μ) that sets where the extremes are centered, a scale parameter (σ>0) that describes how widely they spread, and a shape parameter (ξ) that determines how heavy or bounded the upper tail is.

$$P(Y < y) = GEVD(y|\mu,\sigma,\xi) = exp\{-[1 + \xi\left(\frac{y-\mu}{\sigma}\right)]^{-1/\xi}\} \; with \; \xi \neq 0 \quad (1)$$

Depending on the sign of the shape parameter, the GEVD reduces to the Gumbel, Fréchet or Weibull family. Eq. (1) assumes constant parameters over time, implying a stationary GEVD. To account for the influence of climate change, one or more of the distribution parameters can be allowed to vary as a function of an external covariate. In this study, the GMST is used as a

https://doi.org/10.5194/egusphere-2026-6347
Preprint. Discussion started: 5 November 2026
© Author(s) 2026. CC BY 4.0 License.



covariate to represent the long-term climate change signal. For temperature extremes, the location parameter is modeled as a linear function of GMST, thereby allowing the center of the distribution of extremes to evolve with global warming, whereas, the scale and shape parameters are assumed to remain stationary (Eq. 2a), following previous studies that have shown temporal changes to be primarily reflected in the location parameter (Kharin and Zwiers, 2005; Philip et al., 2020). In contrast, for precipitation extremes, both the location and scale parameters are modeled as exponential functions of GMST (Eq. 2b). This accounts for the expected increase in the variability and intensity of extreme precipitation under a warmer climate, consistent with the thermodynamic constraints imposed by the Clausius–Clapeyron relationship, which predicts an increase of approximately 7% in atmospheric water-holding capacity per degree of warming (Robin and Ribes, 2020). The shape parameter is kept constant in all models. Although temporal changes in the tail behavior cannot be ruled out, reliable estimation of a non-stationary shape parameter generally requires substantially longer records than are typically available (Martins and Stedinger, 2000). Moreover, treating the shape parameter as stationary improves parameter identifiability and facilitates model convergence (Coles, 2001).

$$a)\ \mathcal{M}_{temp}\begin{cases}\mu = \mu_0 + \mu_1 * GMST\\ \sigma = \exp(\sigma_0)\\ \xi = \xi_0\end{cases} \qquad b)\ \mathcal{M}_{pr}\begin{cases}\mu = \mu_0 * \exp(\mu_1 * GMST/\mu_0)\\ \sigma = \exp(\sigma_0 + \sigma_1 * GMST)\\ \xi = \xi_0\end{cases} \tag{2}$$

These GEVD distributions are valid for local applications at individual weather stations. However, to model the distribution parameters spatially, it is necessary to introduce their dependence on geographic covariates, together with a spatial kernel that enables information from nearby stations to be incorporated into the estimation (Davison et al., 2012). The geographic covariates considered in this study are elevation, latitude, longitude, and distance to the sea, all of which were standardized to the range [0, 1] prior to model fitting. This transformation ensures comparability among covariates, improves numerical stability and convergence of the estimation procedure, and facilitates the specification of weakly informative priors on the corresponding coefficients (Gelman et al., 2008). The parameters of the spatio-temporal GEVD are defined according to Eq. (3). Following García et al. (2024), the shape parameter is assumed constant over the entire spatial domain and through time (i.e. a single posterior distribution is estimated jointly for all locations).

$$\begin{aligned}\mu_o(s) &= \mathbb{x}(s)\cdot\alpha_{\mu_0} + W_{\mu_0}(s) + \epsilon_{\mu_0}\\ \mu_1(s) &= \mathbb{x}(s)\cdot\alpha_{\mu_1} + W_{\mu_1}(s) + \epsilon_{\mu_1}\\ \sigma_0(s) &= \mathbb{x}(s)\cdot\alpha_{\sigma_0} + W_{\sigma_0}(s) + \epsilon_{\sigma_0}\\ \sigma_1(s) &= \mathbb{x}(s)\cdot\alpha_{\sigma_1} + W_{\sigma_1}(s) + \epsilon_{\sigma_1}\end{aligned} \tag{3}$$

https://doi.org/10.5194/egusphere-2026-6347
Preprint. Discussion started: 5 November 2026
© Author(s) 2026. CC BY 4.0 License.

where $\mathbb{x}(s)$ is the matrix whose columns contain the geographic covariates, α_k (with $k \equiv \mu_0, \mu_1, \sigma_0, \sigma_1$) are vectors of regression coefficients, and ϵ_k the residuals. The kernel, identified as W_k, is a multivariate Gaussian process with mean $\boldsymbol{0}$ and covariance Σ_k (Eq. 4):

$$W_k(s) \sim MVN(0, \Sigma_k) \tag{4}$$

where the covariance between any two spatial locations s_i and s_j is defined by the exponential covariance function (Eq. 5):

$$\Sigma_k(s_i, s_j) = \beta_{k_1}^2 \exp(-\|s_i - s_j\| / \beta_{k_2}) \tag{5}$$

with $\|s_i - s_j\|$ denoting the Euclidean distance between locations s_i and s_j. The parameter $\beta_{k_1}^2$ is the marginal variance (also known as the process variance), which controls the magnitude of spatial variability, whereas β_{k_2} is the spatial range or decay parameter, which determines how rapidly the correlation decreases with increasing distance between locations (Cooley et al., 2007).

Based on the GEVD, various statistics can be estimated, along with CIs that quantify statistical uncertainty. The T-year return level z_T, representing the magnitude expected to be exceeded, on average, once during T years, is obtained by inverting the GEVD cumulative distribution function at the non-exceedance probability $p = 1 - 1/T$ (Eq. 6, Coles, 2001):

$$z_T = \mu + \frac{\sigma}{\xi}\left[\left(-log\left(1 - \frac{1}{T}\right)\right)^{-\xi} - 1\right], \xi \neq 0 \tag{6}$$

3.2 Bayesian Inference

To estimate the GEVD parameters that best fit the data, we use Bayesian inference, a statistical framework that estimates unknown parameters by updating prior information with the observed data through Bayes' theorem (Etz and Vandekerckhove, 2018; Gelman et al., 2013). It combines three components: the prior, the likelihood, and the posterior. The prior summarizes existing knowledge or assumptions about the model parameters, the likelihood quantifies the probability of observing the data for different parameter values, and the posterior combines these sources of information to provide an updated probability distribution (Ellison, 2004; Karagiannis, 2022). The full hierarchical formulation of the posterior distribution for the spatial GEVD models is provided in Supplementary Material S1.

The posterior distribution of these hierarchical models generally lacks a closed-form solution (Lele et al., 2025; Stringer et al., 2023), necessitating the use of numerical approximation methods to estimate the posterior distribution. Two of the most widely used approaches are the Laplace approximation and MCMC methods. The Laplace approach assumes that the posterior

https://doi.org/10.5194/egusphere-2026-6347
Preprint. Discussion started: 5 November 2026
© Author(s) 2026. CC BY 4.0 License.

distribution can be approximated by a Gaussian distribution centered at its mode, with covariance given by the inverse of the negative Hessian (curvature) at the mode (Rue et al., 2009). This approach is computationally efficient and provides accurate results when the posterior distribution is approximately Gaussian, being unsuitable for multimodal, highly asymmetric, and heavy-tailed posterior distributions (Durante et al., 2024). To assess the validity of this assumption, the approximate posterior distributions were herein evaluated using Mardia's multivariate normality test, which examines multivariate skewness and kurtosis (Mardia, 1980).

Alternatively, MCMC methods generate samples of the true posterior distribution through the convergence of a family of algorithms, without assuming any particular parametric form. As a result, MCMC is asymptotically exact and, despite being computationally more demanding than the Laplace approximation, can faithfully characterize complex posterior features such as multimodality, asymmetry, and heavy tails, even in high-dimensional parameter spaces (Brooks et al., 2011; Gelman et al., 2013). In this study, posterior sampling was performed using the Hamiltonian Monte Carlo algorithm (HMC; Neal, 2011) with the No-U-Turn Sampler (NUTS, Hoffman and Gelman, 2014). HMC enhances sampling efficiency by using the gradient of the log-posterior distribution to propose distant candidate states with high acceptance probabilities, thereby reducing the random-walk behavior that limits the performance of traditional MCMC algorithms. NUTS goes one step further in HMC by changing automatically the trajectory length rather than requiring manual adjustment of this parameter, allowing for efficient exploration of the posterior distribution. Both contribute to lower autocorrelation between draws and are suited to the high-dimensional posterior distributions of hierarchical models. (Carpenter et al., 2017; Hoffman and Gelman, 2014).

The convergence of MCMC models was assessed using two complementary diagnostics: the potential scale reduction factor, which compares the variability between independent MCMC chains with the variability within each chain (Lambert and Vehtari, 2022), with values below 1.01 generally denoting convergence to a common distribution; and the effective sample size, which quantifies the amount of independent information contained in the MCMC samples (Zitzmann and Hecht, 2019), with values exceeding 400 indicating a sufficient number of effectively independent samples. MCMC sampling was tuned separately for each type of extreme, reflecting differences across variables. Precipitation models, which exhibit heavier-tailed posteriors, required a larger number of iterations (e.g., 4,000 warm-up and 10,000 post-warm-up draws per chain), whereas temperature models converged reliably with fewer iterations (4,000 warm-up, and 6,000 sampling).

To implement the Laplace approach and the MCMC algorithms in this study, we used Stan, a freely available probabilistic programming language designed for specifying and fitting Bayesian models (Stan Development Team, 2025). Specifically, the CmdStanR package was used to run Stan from R, which gives access to several inference algorithms (Gabry et al., 2025), facilitating model compilation, sampling, and posterior diagnostics.

3.3 Model Evaluation

To evaluate the goodness of fit and select the model that best fits the data, various metrics were employed. To establish which version of the model (stationary or non-stationary, local or spatial) fits the data best, we applied the Widely Applicable

https://doi.org/10.5194/egusphere-2026-6347
Preprint. Discussion started: 5 November 2026
© Author(s) 2026. CC BY 4.0 License.

Information Criterion (WAIC; Watanabe, 2010). WAIC is a fully Bayesian criterion that estimates how well a model would predict new data, penalizing complexity via an effective number of parameters (Eq. 7, Gelman et al., 2013). Because it is computed from the entire posterior rather than from a single point estimate, WAIC is well suited to hierarchical Bayesian models. Models with lower WAIC values are expected to have better predictive performance and were therefore preferred.

$$WAIC = -2 \cdot lppd + 2 \cdot p_{WAIC} \quad (7)$$

where *lppd* is the log pointwise predictive density, calculated by taking, for each observation, the logarithm of the likelihood averaged over posterior draws and then summing these values across observations; and p_{WAIC} is the effective number of parameters, calculated as the sum, across observations, of the posterior variances of the pointwise log-likelihood contributions (Gelman et al., 2014).

As a complementary tool to WAIC, the Leave-One-Out Probability Integral Transform (LOO-PIT) was also estimated to evaluate how well the model predicts observations not used in the fitting (Gelman et al., 2013; Nguyen et al., 2025). For each observation, the model was refitted without that observation, and the omitted value was then compared with its corresponding posterior predictive distribution (Vehtari et al., 2017). For a well-calibrated model, LOO-PIT values are approximately uniformly distributed, indicating predictive distributions that are neither over- nor under-dispersed and free of systematic bias. Departures from uniformity may point to model misspecification, miscalibrated predictions, or a misrepresentation of uncertainty (Gabry et al., 2019).

Beyond model selection and calibration, goodness-of-fit was assessed using residual analysis, the root mean squared error (RMSE) and the Bayesian *p*-value. Residuals, calculated as the difference between each posterior predictive median and its corresponding observed value, identify systematic biases. The RMSE quantifies the average magnitude of prediction errors by aggregating the squared differences between observed and predicted mean values across all observations, with lower values indicating higher accuracy. The Bayesian *p*-value corresponds to the probability that a chosen test statistic (or discrepancy measure) obtained from each simulated set of GEVD parameters exceeds the same statistic calculated from the observed data (Eq. 8, Gelman et al., 2013). Values close to 0.5 indicate good agreement between the model and the observed data, whereas values near 0 or 1 suggest potential model misspecification or lack of fit.

$$p_B = \Pr(T(y^{rep}, \theta) \geq T(y, \theta) | y) \quad (8)$$

where y represents the observed data, y^{rep} denotes data replicated from the posterior predictive distribution of the fitted model $\mathcal{M}$, and θ represents the vector of GEVD parameters drawn from their posterior distribution. The test statistic $T(y, \theta)$ used in this study is the 90th percentile of the extreme indices, selected to assess the model's ability to reproduce the upper tail behavior of the observed distribution.

https://doi.org/10.5194/egusphere-2026-6347
Preprint. Discussion started: 5 November 2026
© Author(s) 2026. CC BY 4.0 License.

All three metrics were evaluated at the weather stations used for model fitting and at the homogenized stations excluded from the estimation process (Section 2) in order to assess the models' ability to generalize to locations not included in the calibration dataset. Predictions at new stations were derived from the posterior predictive distribution of the fitted spatial GEVD model (Cooley et al., 2007). For each posterior draw, the spatial effect at the new stations was predicted as the sum of (i) a regression term on the geographic covariates at those stations (elevation, latitude, longitude, and distance to the sea) and (ii) the spatially correlated latent effect, obtained from the estimated spatial correlation structure (Eqs. 3–5). Repeating this procedure across all posterior draws yielded a predictive distribution of the model parameters at each new station. The same procedure was used to obtain the parameters of the GEVD on a regular 0.25° × 0.25° grid over peninsular Spain. More details in Supplementary Material S2.

3.4 Universal Kriging

Spatially dependent GEVD models, as described in Section 3.2, are computationally demanding because observations from all weather stations must be modeled jointly. To address this limitation, we evaluated an alternative two-stage approach for obtaining spatially continuous estimates of the GEVD parameters. In this approach, the GEVD parameters are first estimated independently at each weather station using the Bayesian inference models (the Laplace approximation and MCMC sampling). Because each station is modeled separately, parameter estimation depends solely on the local observations, enabling the computations to be performed in parallel and substantially reducing the overall computational burden. In the second stage, the spatial variation of the estimated GEVD parameters is modeled using Universal Kriging with external geographic covariates (Matheron, 2019). The same predictors considered in the spatially dependent GEVD models (elevation, latitude, longitude, and distance to the sea) are incorporated to interpolate the locally estimated parameters across the study domain. To propagate parameter uncertainty through the spatial interpolation, Universal Kriging was applied to the posterior samples of the GEVD parameters. The location parameter and the logarithm of the scale parameter were interpolated in this manner. The shape parameter ξ, in contrast, was assumed to be spatially homogeneous, as in the spatial GEVD models of Section 3.1, and a single regional value was obtained by pooling the station-level posterior draws (following García et al., 2024). This choice is motivated by the fact that station-level shape estimates are usually poorly constrained given the limited number of extreme observations per station, and interpolating such unstable estimates would propagate this noise into the resulting map (Martins and Stedinger, 2000). To account for uncertainty in this parameter, one posterior draw of the shape parameter was randomly sampled from each station, and the median of these station-specific draws was computed. This procedure was repeated for all posterior realizations, yielding a posterior distribution for the regional shape parameter. The universal kriging method used to interpolate parameter estimates to unobserved locations is further described in Supplementary Material S3.

https://doi.org/10.5194/egusphere-2026-6347
Preprint. Discussion started: 5 November 2026
© Author(s) 2026. CC BY 4.0 License.

4 Results

Before fitting the GEVD, we assessed whether temperature and precipitation extremes exhibit a significant relationship with GMST. This preliminary analysis provides insight into the behavior of extremes as a function of global warming and motivates the need to account for non-stationarity in the GEVD formulation. Figure 1 reveals contrasting patterns for temperature and precipitation extremes. Across peninsular Spain, summer temperature extremes exhibit widespread and statistically significant positive relationships with GMST. On average, TXx rises by 2.7 °C for every 1 °C of GMST warming, indicating a substantially stronger response in summer temperature extremes compared with the global mean. The magnitude of this response is consistent with the broader context of rapid warming across Europe, which has warmed at more than twice the global average since the 1980s, with summer warming particularly pronounced across western Europe (C3S/ECMWF and WMO, 2026). In contrast, precipitation extremes show mixed linkages, with both positive and negative slopes, which is consistent with an overall lack of significant changes in precipitation extremes, as also reported in recent studies (Beguería et al., 2025).

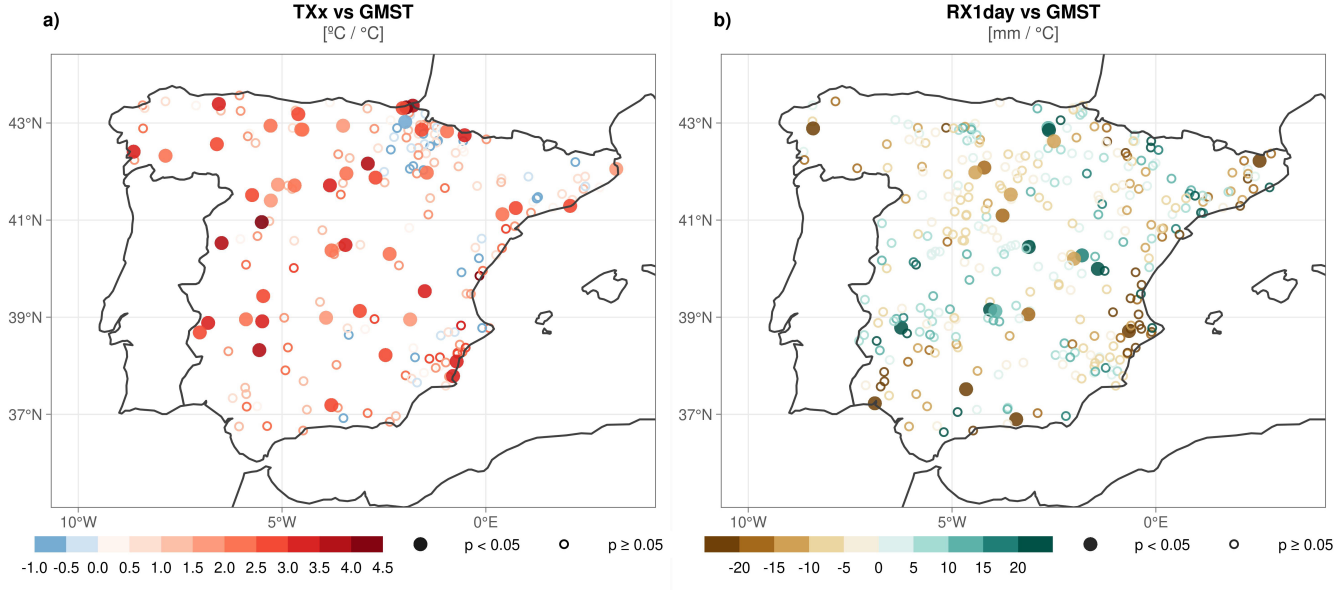


Figure 1: Relationship of summer temperature extremes (a) and autumn precipitation extremes (b) with global mean surface temperature (GMST) over the period 1981-2022. Associations were estimated using generalized least squares regression with an AR(1) correlation structure to account for temporal autocorrelation. Significant associations ($p < 0.05$) are indicated by solid circles, whereas non-significant trends are shown as open circles.

4.1 Daily Extreme Temperatures

We considered four GEVD formulations for summer TXx, differing in whether GMST is included as a covariate (stationary vs. non-stationary) and whether spatial information is incorporated (local vs. spatial). To compare model fit and predictive performance, the four GEVD models (fitted via MCMC) were evaluated using the WAIC and the LOO-PIT (Figure 2).

https://doi.org/10.5194/egusphere-2026-6347
Preprint. Discussion started: 5 November 2026
© Author(s) 2026. CC BY 4.0 License.

Comparing local and spatial formulations, spatial models achieve the lowest WAIC far more often than their local counterparts (Figure 2a–d). On the other hand, stationary versus non-stationary formulations reveal a clearer benefit of including GMST as a covariate, with the non-stationary spatial models yielding lower WAIC values at many stations, particularly across the central-western Iberian Peninsula (Figure 2d). This is consistent with the stronger GMST scaling observed in these regions (Figure 1). The spatial models further show uniform LOO-PIT distributions and are better calibrated than their local counterparts (Figure 2e-h). The non-stationary local model shows the most severe miscalibration, with a marked excess of LOO-PIT values near 0, indicating that the predictive distributions tend to overestimate the magnitude of the most extreme events (Figure 2g). Taken together, these results indicate that both spatial dependence and non-stationarity contribute meaningfully to improved model fit and predictive calibration. The improvement associated with the spatial formulation, in turn, likely reflects the information shared among neighboring stations through the spatial covariance structure. By borrowing strength across sites, the spatial models regularize parameter estimates, reducing their sensitivity to local sampling variability and limiting the influence of individual observations (Cooley et al., 2007; Sang and Gelfand, 2010). This provides greater robustness under cross-validation than the local models, whose estimates depend exclusively on station-specific data (Davison et al., 2012; Vehtari et al., 2017).

Using the Laplace approximation to infer the GEVD parameters yields conclusions similar to those obtained with MCMC, while substantially reducing the computational cost (Figure S1 and Table S1). However, the GEVD parameters of the spatial models deviate significantly from a multivariate normal distribution as compared to those obtained via MCMC, according to Mardia's test. This departure from multivariate normality does not necessarily manifest in the LOO-PIT diagnostics, which remain well calibrated under the Laplace approximation. Nevertheless, this approximation may still have important consequences: CIs for parameters may be poorly represented (Rue and Martino, 2007), and the joint dependence structure among parameters may not reflect the true posterior correlation structure (Figure S2). This is of particular concern for return-period computations, where the uncertainty in the GEVD parameters propagates into the estimated return levels. Accordingly, subsequent analyses of temperature extremes focus on the non-stationary spatial GEVD fitted via MCMC, while the Laplace approximation is only used for comparison purposes to assess the strengths and limitations of this fast assessment.

Having identified the non-stationary GEVD as the preferred configuration, we next assess whether this model provides an adequate absolute fit to the observed data (Figures S3-S4). Overall, the residuals are centered close to zero across all stations, indicating no systematic tendency to overestimate or underestimate TXx in any region (Fig. S3a, d). The RMSE is generally low, remaining below 3 °C, with the largest errors occurring in coastal areas, where interannual variability is also the largest (Fig. S3b, e). Likewise, the 90th percentile of TXx is accurately reproduced, with no evidence of substantial regional biases (Fig. S3c, f). These results are consistent across modeling approaches (local and spatial models), and inference methods (Laplace approximation and MCMC; cf. Figs. S3 and S4), supporting the robustness of the fit.

https://doi.org/10.5194/egusphere-2026-6347
Preprint. Discussion started: 5 November 2026
© Author(s) 2026. CC BY 4.0 License.

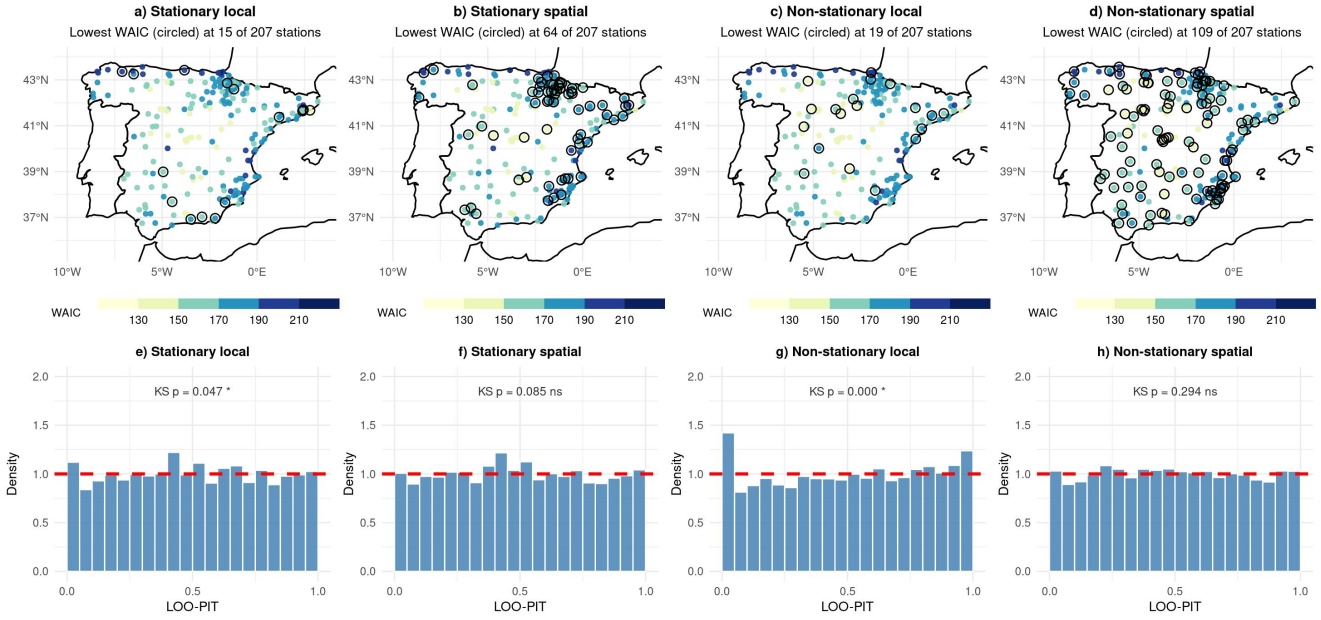


Figure 2: Comparison of four GEVD formulations for summer extreme temperatures (TXx): stationary local, stationary spatial, non-stationary local, and non-stationary spatial, with parameters estimated at 207 weather stations via MCMC Bayesian inference. Top row (a-d): Widely Applicable Information Criterion (WAIC). Black circles mark stations where that model attains the lowest WAIC among the four, and the number of such stations relative to the total is reported above each panel. Bottom row (e-h): LOO-PIT histograms for each of the four models, assessing calibration of the leave-one-out posterior predictive distributions. Under perfect calibration, LOO-PIT values are uniformly distributed (red dashed line); deviations from uniformity are formally tested with the Kolmogorov–Smirnov (KS) test, reported for each panel.

The parameters of GEVD are shown in Figure 3. The location intercept μ_0 can be interpreted as the characteristic extreme temperature at a reference location. Accordingly, the highest values exceeding 40 °C are found in southern Spain (Andalusia) and in the northeast (the Ebro Valley), whereas the lowest values occur in the northwest of the country (Fig. 3a, e), consistent with climatological assessments (Chazarra Bernabé et al., 2018). The dependence on GMST, represented by μ_1, differs between the local and the spatial GEVD models (Fig. 3b, f). The local estimate yields slopes with substantial variation between nearby stations, similar to the scaling pattern of Fig. 1. Spatial aggregation smooths out the association while preserving the overall spatial structure, characterized by slopes in summer TXx above 2°C per degree of global warming in central-western Spain, and non-significant associations in the northeast. The smoothing effect of the spatial model is expected because neighboring stations share information through the spatial dependence structure, reducing sampling variability. The scale parameter exhibits a clear and robust spatial gradient, with markedly higher variability in summer TXx along the Mediterranean and Cantabrian coast and Ebro valley compared to the central plateau (Fig. 3c, g). The shape parameter ξ, represented by a single pooled estimate across the entire domain in the spatial model, is negative and significantly different from zero, consistent with the dominance of negative ξ values under the local formulation (Fig. 3d, h). Negative ξ implies a finite upper endpoint of the GEVD, indicating that summer temperature extremes are physically bounded.

https://doi.org/10.5194/egusphere-2026-6347
Preprint. Discussion started: 5 November 2026
© Author(s) 2026. CC BY 4.0 License.

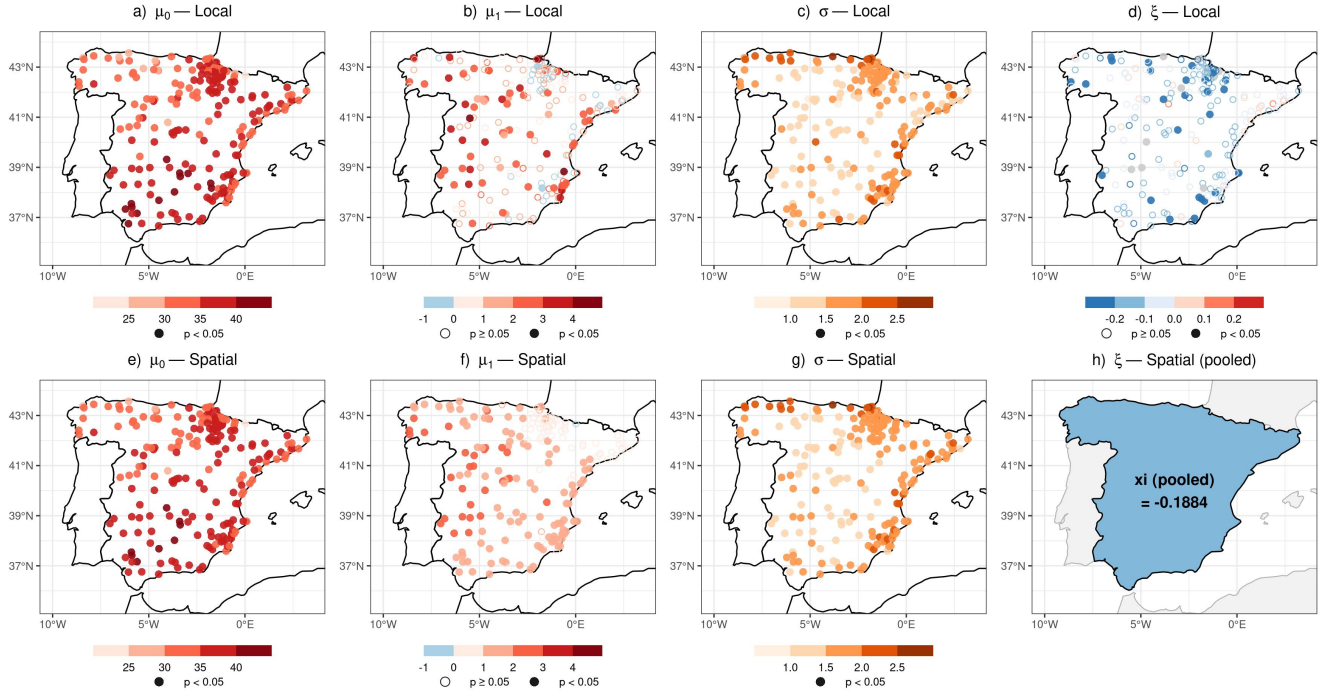


Figure 3: Spatial distribution of GEVD parameters for summer extreme temperatures (TXx) estimated via the MCMC, comparing local (top row, a-d) and spatial (bottom row, e-h) model formulations. Columns show, from left to right, the location intercept ($\mu_0, °C$) (a, e), the GMST-trend coefficient ($\mu_1, °C/°C$) (b, f), the scale parameter ($\sigma, °C$) (c, g), and the shape parameter (ξ) (d, h). Color indicates the posterior mean at each station; solid circles denote stations where the 95% credible interval (CI) excludes zero (statistically significant), while open circles denote non-significant estimates. Because the shape parameter is treated as spatially homogeneous in the spatial formulation (see Methods), the corresponding panel reports a single pooled posterior estimate rather than a station-based map.

The GEVD parameters estimated using the Laplace approximation yield fairly similar results overall. The most notable difference arises in μ_1 under the spatial formulation: the Laplace approximation smooths the trend field more strongly than MCMC, yielding significant positive slopes in the northeast of the country, in contrast to the non-significant MCMC estimates (Figure S5).

The spatial model incorporates the dependence of the GEVD parameters on geographic covariates (Eq. 3), which captures the influence of topographic and climatic factors on the spatial variability of extreme events (Table 1). Overall, the relationships between the GEVD parameters and the geographic covariates are modest, and mainly imply μ_0. The clearest effect concerns the decreases of μ_0 with altitude at a rate of approximately 4.34°C/km, consistent with García et al. (2024). The effect of continentality is also apparent: inland stations exhibit warmer average extreme conditions than those near the coast, consistent with the moderating influence of the ocean on temperature. In addition, there is a negative latitudinal gradient in μ_0, indicating that extreme values tend to decrease with increasing latitude, although this effect is only statistically significant under the Laplace approximation (Table S2). On the other hand, long-term changes in TXx (as inferred from μ_1) are not systematically modulated by elevation, latitude, or continentality at the national scale, which is consistent with the results of García et al.

https://doi.org/10.5194/egusphere-2026-6347
Preprint. Discussion started: 5 November 2026
© Author(s) 2026. CC BY 4.0 License.

(2024). The only significant relationship with μ_1 is a negative effect of longitude under the Laplace approximation, indicating that μ_1 decrease from west to east (Table S2). Concerning the shape parameter, the variability of summer TXx is greater along the coast and decreases toward the interior of the peninsula, as noted earlier.

Parameter	Intercept	Elevation (km)	Longitude (°)	Latitude (°)	Coast distance (km)
μ_0 ($°C$)	**58.51 (22.69; 88.30)**	**-4.34 (-5.32; -3.37)**	0.03 (-0.50; 0.55)	-0.63 (-1.35; 0.23)	**0.03 (0.01; 0.04)**
μ_1 ($°C$ / $°C$)	5.57 (-2.40; 13.37)	-0.40 (-1.01; 0.19)	-0.12 (-0.26; 0.02)	-0.07 (-0.26; 0.13)	0.002 (-0.002; 0.005)
σ ($°C$)	-0.69 (-3.33; 1.83)	-0.06 (-0.18; 0.06)	-0.008 (-0.052; 0.036)	0.04 (-0.03; 0.10)	**-0.001 (-0.002; -2.88e-5)**

Table 1: Posterior mean estimates of the regression coefficients relating the GEVD location (μ_0, μ_1) and scale (σ) parameters to geographic covariates, under the non-stationary spatial GEVD model of summer TXx fitted via MCMC. Row labels indicate the unit of the corresponding GEVD parameter, and column headers indicate the unit of the covariate; the unit of each coefficient is therefore the ratio of the two. Bold values indicate coefficients whose 95% CI excludes zero.

We next assess the out-of-sample predictive performance of the GEVD model at stations that were not included in the fitting process. This evaluation is essential for determining the model's ability to characterize extreme temperatures at ungauged locations, where observations are unavailable. To this end, the GEVD parameters at the validation temperature stations (Section 2) were predicted using either the spatial MCMC model or the two-step approach. The predictive performance was then evaluated with a range of goodness-of-fit metrics to assess the accuracy and reliability of the spatial interpolation. Although the spatial patterns are similar, the comparison of the two interpolation approaches indicates that the fully Bayesian method exhibits superior performance, as evidenced by smaller residuals, lower RMSE values, and a greater proportion of stations where the 90th percentile is more accurately estimated (Figure 4 and Figure S6). The largest errors are concentrated along the northern and southern coastlines (Figure 4b, e), where the models systematically overestimate TXx (Figure 4a, d). This pattern likely reflects an underestimation of the sea's moderating influence, which is not observed along the eastern Mediterranean coast, where the marine influence seems to be well resolved by the distance-to-sea covariate. This discrepancy may be explained by differences in sea surface temperature: the northern and southern coasts are influenced by cooler waters than the Mediterranean, resulting in a stronger cooling effect on nearby TXx values that is not fully captured by a single, spatially uniform distance-to-sea relationship. Furthermore, the 90th percentile is not adequately reproduced at approximately 40% of the stations in the fully Bayesian model, with underestimation and overestimation occurring in nearly equal proportions (Figure 4c, f). Despite these limitations, this model predicts TXx across the interior of the peninsula with errors of approximately 2°C, comparable to those obtained at the stations used for model calibration (Figs. S3-S4).

https://doi.org/10.5194/egusphere-2026-6347
Preprint. Discussion started: 5 November 2026
© Author(s) 2026. CC BY 4.0 License.

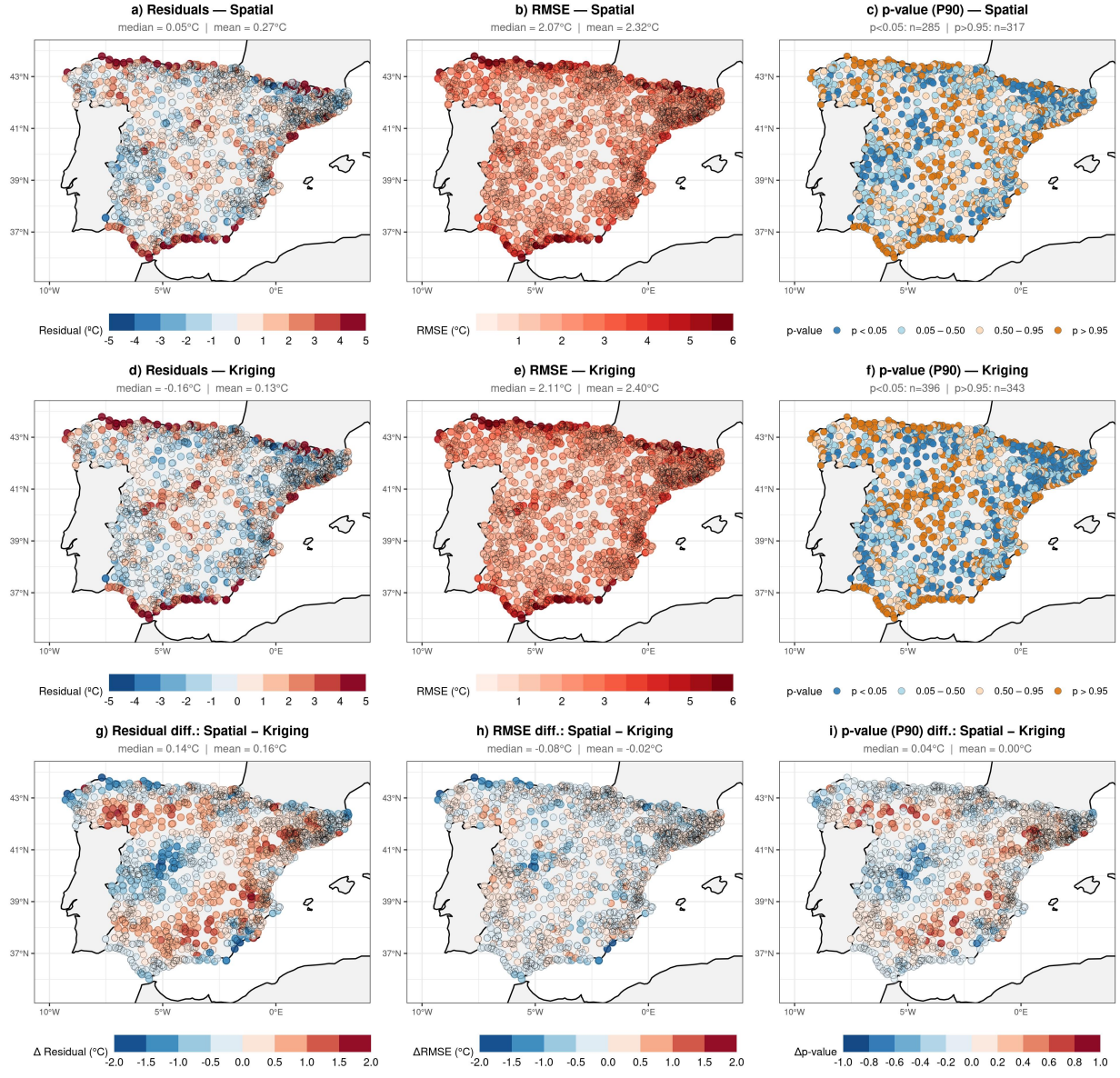


Figure 4: Predictive performance of summer TXx at stations excluded from the model fitting for the fully Bayesian spatial model using MCMC and kriging interpolation of the Bayesian local model. Rows show, from top to bottom: the spatial model (a, b, c), kriging (d, e, f), and their difference (Spatial − Kriging) (g, h, i). Columns show, from left to right: point-level residuals (predicted − observed median, °C) (a, d, g), root-mean-square error (RMSE, computed using the predicted mean, °C) (b, e, h), and Bayesian posterior predictive p-values for the 90th percentile, classified into four categories (p<0.05, [0.05, 0.5), [0.5, 0.95], p>0.95) to flag stations with poor predictive performance. Summary statistics (mean and median) are reported above each panel, along with counts of stations (n) falling in the extreme p-value categories.

https://doi.org/10.5194/egusphere-2026-6347
Preprint. Discussion started: 5 November 2026
© Author(s) 2026. CC BY 4.0 License.

Based on the good predictive performance, the two spatial approaches were also applied to estimate the GEVD parameters on a regular 0.25° grid covering the peninsula (Figures S7–S9) and to derive the corresponding 100-year return levels (RL100) under different warming scenarios (Figure 5). The highest return levels occur in southwestern Spain, particularly in the Guadalquivir Valley, and in the Ebro Valley in the northeast, consistent with the regions experiencing the warmest temperature extremes on the Iberian Peninsula. As GMST rises, the spatial mean of the estimated 100-year return levels (RL100) of summer TXx across peninsular Spain increases faster than GMST, indicating an amplified warming response (Fig. 5). Under preindustrial conditions (GMST anomaly of 0 °C), the spatial mean RL100 is estimated at 40.5 °C (Fig. 5a, d). At a GMST anomaly of 1.3 °C, it reaches approximately 42.5 °C, an increase of about 2 °C (Fig. 5b, e). At 2.5 °C of global warming, the spatial mean RL100 reaches 44.3 °C, with local estimates approaching 50 °C in southwestern Spain (Fig. 5c, f). The 2.5°C warming scenario was selected based on projections reported by the United Nations Environment Programme (UNEP, 2025), which indicate that current global emission trajectories are consistent with approximately this level of warming by the end of the century.

Results obtained using universal kriging show broadly similar mean estimates, but the two approaches diverge substantially in their quantification of uncertainty (Fig. 5g-i). CIs for the return levels obtained from universal kriging are considerably wider than those from the fully Bayesian model, reflecting the wider intervals already present in kriging's estimation of the GEVD parameters (Figs. S7–S9). The lower uncertainty of the fully Bayesian model is consistent with neighboring locations sharing information within a single spatial model. Narrower intervals are useful in practice, since climate risk assessment and adaptation planning rely on accurate estimates of rare events.

4.2 Daily Extreme Precipitations

Following the same approach adopted for the extreme temperatures, we first assessed the performance of the candidate models for the autumn Rx1day data using the WAIC and LOO-PIT diagnostics. Overall, the spatial formulations yielded lower WAIC values than their local counterparts under MCMC inference (Fig. 6a–d), and this advantage was substantially greater when model comparison was conducted using the Laplace approximation (Fig. S10). Among the spatial models, the stationary formulation attained the lowest WAIC at more stations than the non-stationary formulation (Fig. 6b, d). In line with these results, very few stations exhibit significant slopes in autumn Rx1day (Fig. 1), matching previous studies that found no significant trend in precipitation extremes in the country (Beguería et al., 2025). The stationary spatial model also shows better predictive performance than the local model, being the only formulation whose LOO-PIT distribution does not differ significantly from a uniform distribution (Fig. 6e-h). Overall, WAIC and LOO-PIT point to the stationary spatial model as the most appropriate representation of autumn Rx1day in Spain, as it combines improved fit and predictive performance. As observed in TXx, the Laplace approximation has some difficulty in representing the parameters associated with the spatial kernel (Figure S11). This is consistent with a Mardia's test, indicating that the joint posterior of these parameters departs from multivariate normality — an assumption the Laplace approximation relies on. Therefore, we adopt MCMC as the inference method for the spatial hyperparameters throughout this study, using the Laplace approximation only for model comparison.

https://doi.org/10.5194/egusphere-2026-6347
Preprint. Discussion started: 5 November 2026
© Author(s) 2026. CC BY 4.0 License.

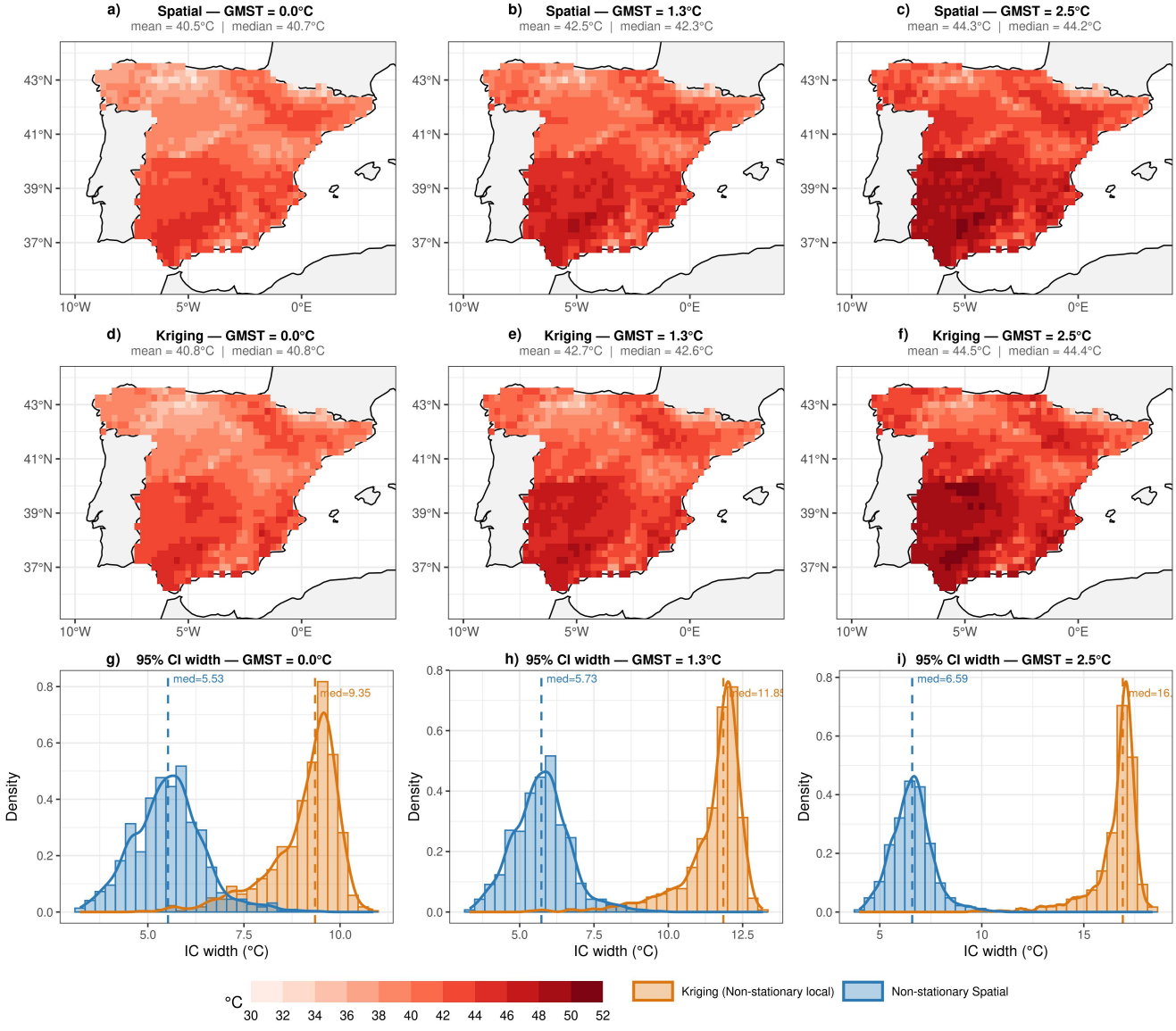


Figure 5: Comparison of 100-year return levels (RL100) of summer TXx between the fully Bayesian spatial model (top row, a-c) and universal kriging (middle row, d-f) across three global mean surface temperature (GMST) scenarios: preindustrial (0.0°C global warming, left), present-day (1.3°C global warming, center), and a 2.5°C warmer world (right). The bottom row (g-i) shows the corresponding distributions of 95% credibility interval (CI) width for RL100 under each scenario, comparing the spatial model (blue) against kriging (orange); dashed vertical lines mark the median CI width for each method.

While WAIC and LOO-PIT provide a basis for model selection according to predictive performance, they do not by themselves indicate how closely the selected model reproduces the observed record. Goodness of fit was assessed using posterior predictive replicates of the GEVD (Figures S13–S14). Unlike TXx, the two spatial approaches diverge in the residuals: local

https://doi.org/10.5194/egusphere-2026-6347
Preprint. Discussion started: 5 November 2026
© Author(s) 2026. CC BY 4.0 License.

models tend to underestimate precipitation extremes at almost all stations, whereas the full spatial Bayesian model both underestimates and overestimates Rx1day without a specific spatial pattern (Fig. S13a, d). This is consistent with the well-documented finite-sample properties of extreme value estimators, which produce a systematic negative bias in the shape parameter for relatively short series, propagating into underestimated upper quantiles (Carney, 2016; Goda, 2011). This effect is particularly important in precipitation extremes, as they already exhibit greater asymmetry and sample variance than temperature extremes. The spatial Bayesian model mitigates this systematic bias through partial pooling: each station's posterior is informed by the regional structure via the spatial Gaussian process, which reduces the directional bias observed in the local fits (Cooley et al., 2007; Sang and Gelfand, 2010; Renard, 2011). As expected from the magnitude and variability of extremes (Fig. 7), the RMSE reaches its highest values along the Mediterranean coast, with no substantial differences between the two modeling approaches (Figs. S13-S14b, e). Meanwhile, the 90th percentile of Rx1day is generally well captured at most stations, although the local approach shows a slight tendency to underestimate this quantile, consistent with the residual analysis (Fig. S13c, f).

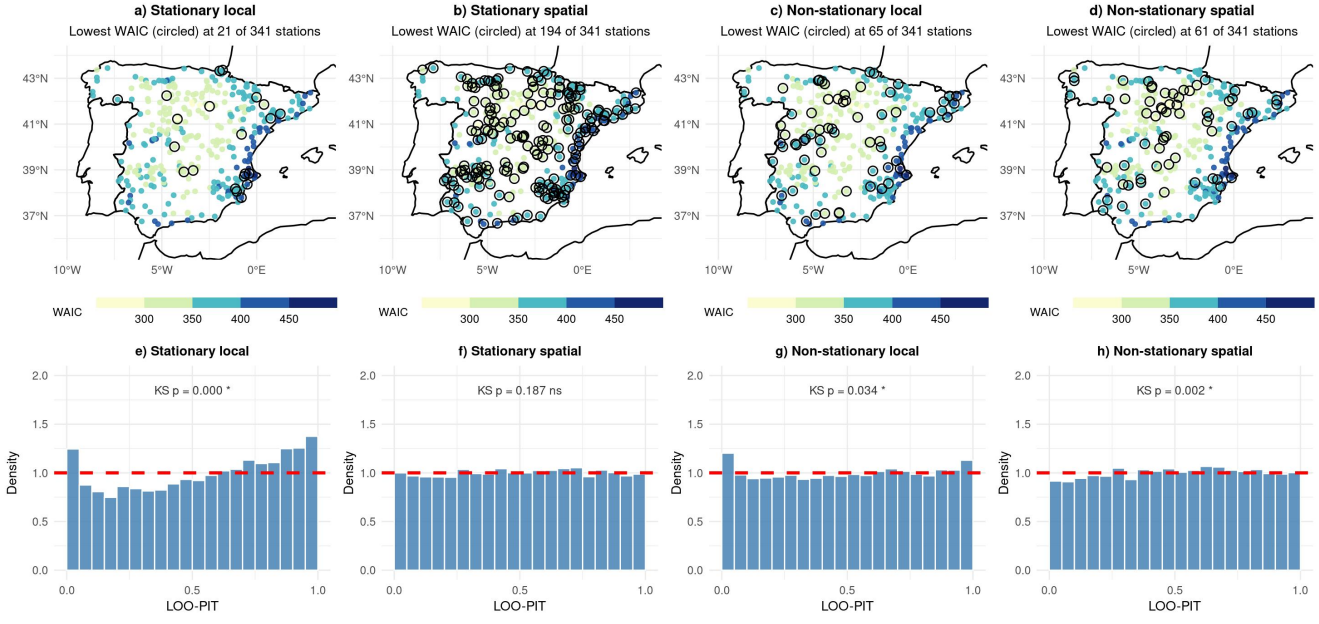


Figure 6: Same as Fig.2 but for extreme autumn precipitation (RX1day).

The parameters of the chosen GEVD are shown in Figure 7. The location parameter, μ_0, indicates that precipitation extremes are most intense at Mediterranean coastal stations and at several stations in the north of the country, with the lowest values found in the central plateau, consistent with the spatial structure of autumn RX1day (Gonzalez-Hidalgo et al., 2025). As in summer TXx, the spatial model produces a smoother, more spatially coherent representation of precipitation extremes along the Mediterranean coast than the local fits (Fig. 7a, d). The scale parameter σ shows greater interannual variability at

https://doi.org/10.5194/egusphere-2026-6347
Preprint. Discussion started: 5 November 2026
© Author(s) 2026. CC BY 4.0 License.

Mediterranean stations, consistent with their frequent exposure to intense convective events during autumn (Ferreira, 2021). Finally, the shape parameter ξ is positive, consistent with the dominance of positive values across the local fits, indicating an unbounded upper tail of the GEVD. The spatial patterns of the parameters estimated using the Laplace approximation are very similar to those obtained via MCMC (Figure S12).

The analysis of the stationary spatial GEVD parameters and the geographic covariates reveals that both the location and scale of precipitation extremes depend on elevation and distance to the sea (Table 2). RX1day values are more intense and more variable at higher-elevation stations than at lower-elevation ones. Likewise, inland stations exhibit weaker and less variable extremes than coastal stations. The Laplace approximation leads to the same overall conclusions (Table S3).

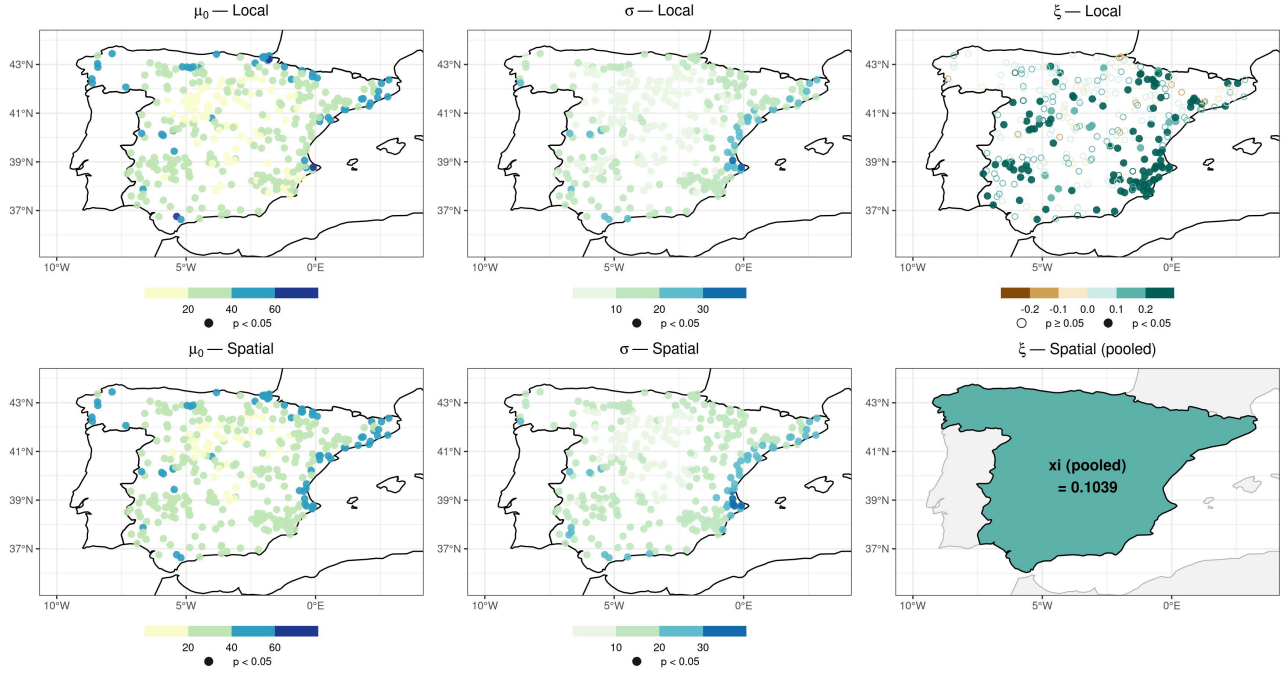


Figure 7: Same as Fig. 3 but for autumn extreme precipitations (Rx1day) and the stationary GEVD model, with columns showing the location intercept (μ_0, mm) (a, d), the scale parameter (σ, mm) (b, e), and the shape parameter (ξ) (c, f).

Parameter	Intercept	Elevation (km)	Longitude (°)	Latitude (°)	Coast distance (km)
μ_0 (mm)	-49.41 (-129.86; 28.91)	**8.75 (5.92; 11.55)**	0.80 (-0.49; 2.12)	1.83 (-0.16; 3.87)	**-0.0348 (-0.0690; -0.0003)**
σ (mm)	**3.51 (0.00; 6.82)**	**0.19 (0.05; 0.32)**	0.10 (-0.06; 0.27)	-0.02 (-0.11; 0.06)	**-9.33e-4 (-1.41e-3; -4.49e-4)**

Table 2: As Table 1 but for the GEVD location (μ_0) and scale (σ) parameters under the stationary spatial GEVD model fitted via MCMC for autumn Rx1day.

The model's predictive performance at unseen stations was evaluated by using extreme precipitation data from the verification weather stations excluded from the fitting process (Section 2). The results reveal a spatially heterogeneous pattern, with the largest absolute residuals of Rx1day occurring in the northwestern and central-western regions for both interpolation

https://doi.org/10.5194/egusphere-2026-6347
Preprint. Discussion started: 5 November 2026
© Author(s) 2026. CC BY 4.0 License.

approaches (Figure 8 and Figure S15). The main difference between the two interpolation approaches occurs along the Mediterranean coast, where the fully Bayesian spatial model generally overestimates extremes, whereas universal kriging tends to underestimate them, reflecting the local model's underestimation of Rx1day (Fig. 8a, d, g). The RMSE pattern is very similar for both approaches, with the largest prediction errors concentrated in the eastern part of the country (Fig. 8b, e, h). These predictive RMSE values are comparable to those obtained at the stations used to calibrate the models, suggesting the spatial model generalizes well to unsampled locations. The 90th percentile preserves the pattern observed in the residuals: the full spatial Bayesian model more frequently overestimates the percentile, whereas kriging tends toward underestimation (Fig. 8c, f, i). Unlike the TXx results, kriging outperforms the fully Bayesian model in capturing the 90th percentile of autumn Rx1day across Spain, although the fully Bayesian model performs better in regions prone to heavy precipitation such as the Mediterranean coast.

Finally, we estimated the RL100 of Rx1day on a uniform 0.25° grid across Spain (Figure 9). Both interpolation approaches reproduce broadly similar spatial patterns, with the highest return levels concentrated along the Mediterranean coast and in the northwest, and comparatively lower values over the central plateau (Fig. 9a, b). The fully spatial Bayesian model yields slightly higher estimates than kriging, consistent with the residual analyses above. In contrast to summer TXx, the uncertainty in the RL100 estimates for autumn Rx1day (quantified by the CI width) is comparable between the two approaches (Fig. 9c), with kriging displaying only slightly wider intervals due to larger uncertainty in the GEVD parameters, particularly for the location parameter (Figures S16-S17). Although these differences are modest, they can have consequences in infrastructure design, where small changes in estimated return levels may substantially affect safety margins and costs.

https://doi.org/10.5194/egusphere-2026-6347
Preprint. Discussion started: 5 November 2026
© Author(s) 2026. CC BY 4.0 License.

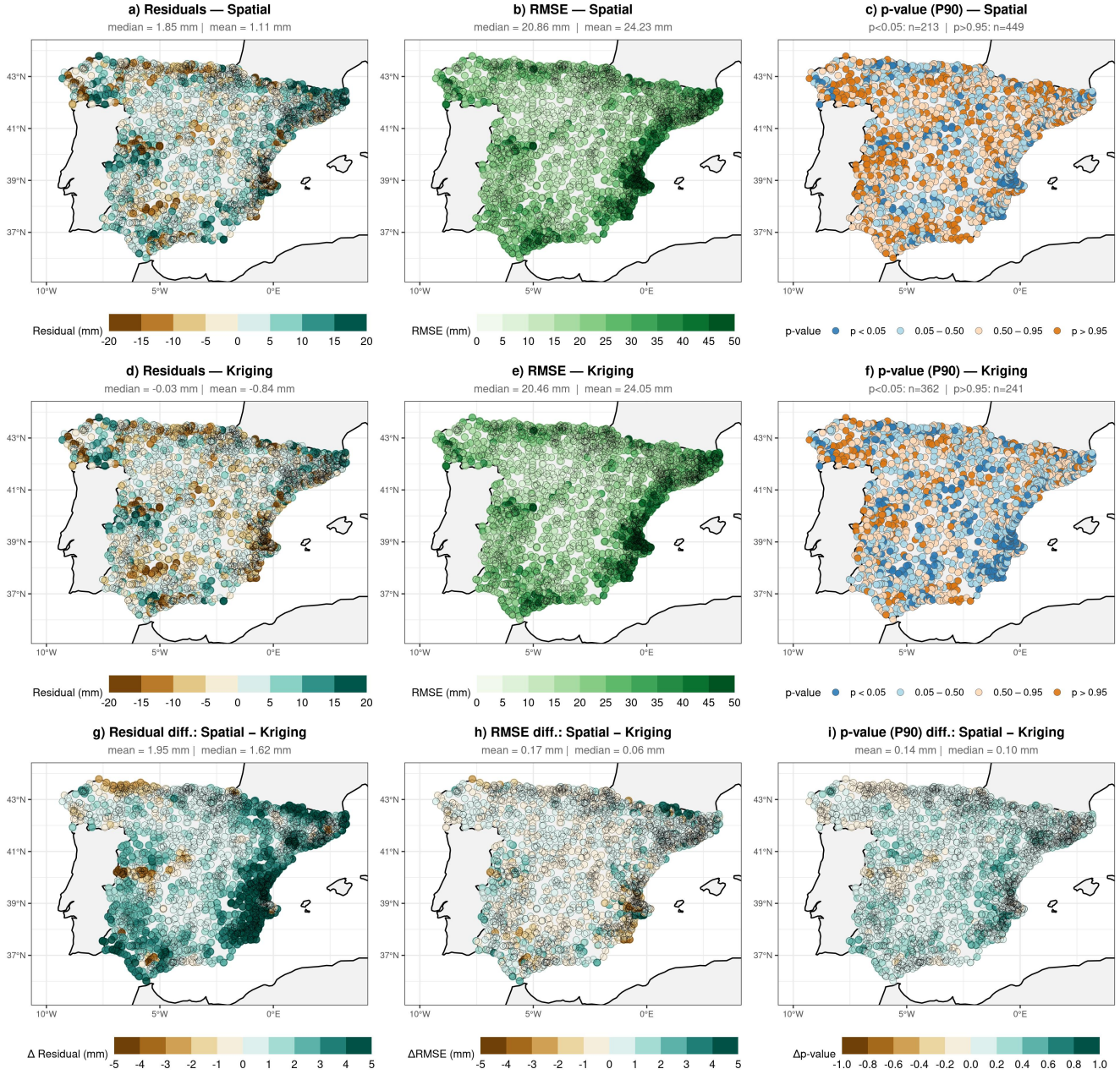


Figure 8: As Fig. 4 but for autumn Rx1day and the stationary versions of the fully Bayesian spatial model using MCMC and kriging interpolation of the Bayesian local model.

https://doi.org/10.5194/egusphere-2026-6347
Preprint. Discussion started: 5 November 2026
© Author(s) 2026. CC BY 4.0 License.

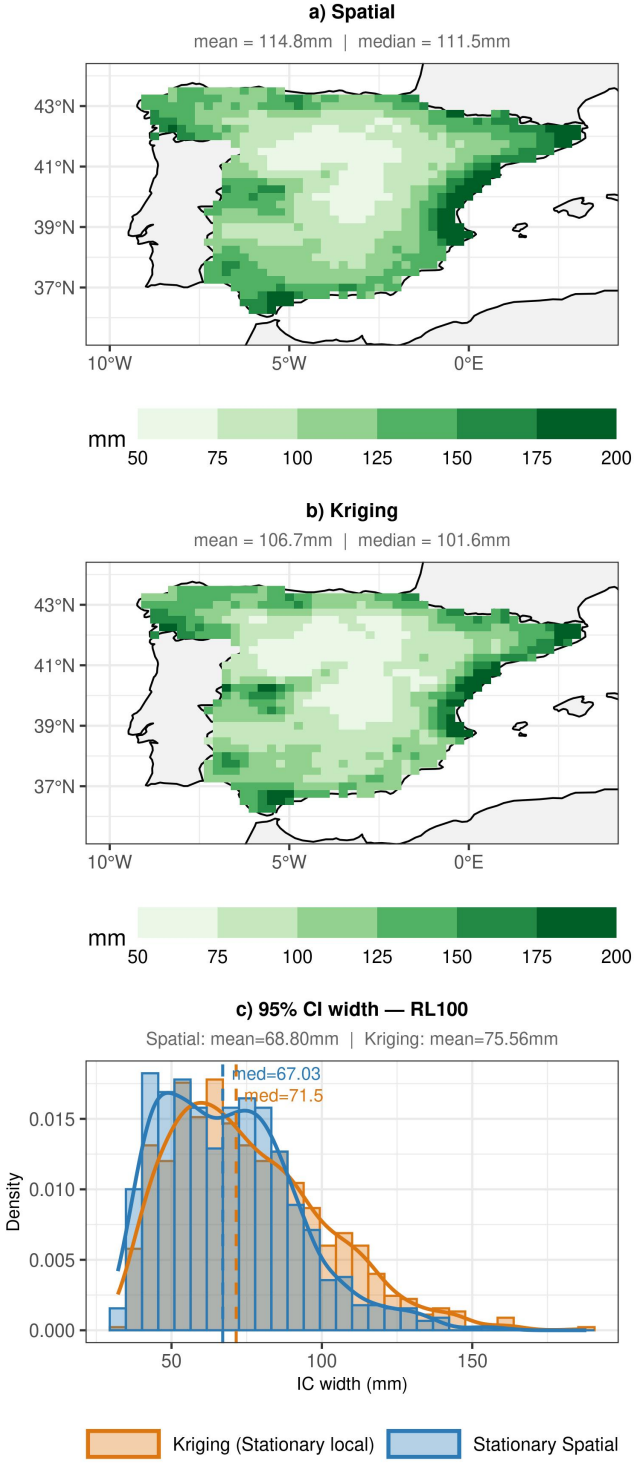


Figure 9: Same as Fig. 5 but for the stationary RL100 of autumn Rx1day.

https://doi.org/10.5194/egusphere-2026-6347
Preprint. Discussion started: 5 November 2026
© Author(s) 2026. CC BY 4.0 License.

5 Discussion

A key finding of this study is the contrasting non-stationary behavior of summer daily temperature extremes (TXx) and autumn daily precipitation extremes (Rx1day) over peninsular Spain. The pronounced non-stationary signal identified for TXx, particularly over western Spain, indicates that the temporal evolution of temperature extremes cannot be adequately represented by a stationary model over the study period. At most stations incorporating a climate change covariate improves their representation. Moreover, we found that TXx increased faster than GMST itself, indicating an amplification of summer temperature extremes in Spain relative to global warming, which is consistent with accelerated trends across western Europe (Vautard et al., 2023; García et al., 2024; C3S/ECMWF and WMO, 2026). Part of this amplification is expected a priori, since GMST is a global, ocean-dominated index, whereas TXx is measured exclusively over land. Because continental surfaces respond more strongly than the ocean to radiative forcing, particularly in summer, a stronger response over Spain relative to GMST is therefore plausible (Joshi et al., 2008). This land–sea contrast is further reinforced where soil moisture becomes limiting, as reduced evapotranspiration lowers boundary-layer relative humidity and amplifies surface warming (Joshi et al., 2008; Seneviratne et al., 2010). In contrast, autumn daily precipitation extremes are generally well described by stationary models, suggesting that long-term trends in rainfall extremes are weak compared with natural variability over the study period. This asymmetry mirrors the different physical mechanisms governing the two types of extremes. While temperature extremes are shaped by atmospheric dynamics, their long-term trends are heavily dominated by the direct radiative forcing of increasing greenhouse gas concentrations, which warms the troposphere and Earth's surface and increases the frequency and intensity of warm extremes almost everywhere (IPCC AR6, 2023). Precipitation extremes, by contrast, involve a much stronger interplay between thermodynamic constraints (e.g. Clausius-Clapeyron) and dynamic drivers like atmospheric circulation, moisture transport, and mesoscale convection (e.g. Andria et al., 2025), resulting in greater spatial heterogeneity and making long-term changes more difficult to detect at regional scales (O'Gorman, 2015).

Incorporating spatial structure improves the representation of both variables, although its benefits depend on the complexity of the underlying process. For TXx, the fully spatial Bayesian model consistently outperforms the two-step kriging approach, with the difference becoming more pronounced in the non-stationary formulation because uncertainty in both the climate-related trend and the spatial covariance must be propagated jointly. By interpolating each GEVD parameter independently, kriging does not retain the joint dependence structure established during the local fits, resulting in systematically wider confidence intervals. For Rx1day, however, the stationary formulation involves a simpler uncertainty structure, and decoupling the interpolation step therefore has a smaller impact: the two approaches produce similar confidence-interval widths, with kriging only marginally wider. These results indicate that the value of a fully spatial model depends not only on the presence of spatial dependence, but also on the complexity of the process and parameter uncertainty being estimated.

https://doi.org/10.5194/egusphere-2026-6347
Preprint. Discussion started: 5 November 2026
© Author(s) 2026. CC BY 4.0 License.

An alternative strategy, commonly adopted in earlier hydrological literature, interpolates return levels directly rather than the GEVD parameters: the distribution is fitted independently at each station, the return level of interest (e.g., the 50- or 100-year event) is estimated locally, and the resulting scalar field is then interpolated using kriging (Szolgay et al., 2009). However, this approach treats each return period as an independent spatial variable, ignoring the fact that all return levels are derived from the same underlying probability distribution. Consequently, it can produce internally inconsistent return-level maps and does not permit the propagation of uncertainty arising from the estimation of the GEVD parameters (Roksvåg et al., 2021). Our findings underscore the benefits of explicitly modelling spatial structure, consistent with previous studies reporting similar advantages for other hazards. For example, Blanchet and Lehning (2010) found that a fully spatial GEVD model outperformed local fitting followed by interpolation when producing snow-depth hazard maps for structural design and avalanche risk management in the Alps.

Beyond its effect on predictive performance, spatial formulation provides insight into the geographic controls of extreme-event distributions. For summer TXx, the spatial variation in the magnitude of extreme temperatures reflects broad topographic and maritime gradients. However, the GMST scaling parameter shows no systematic dependence on the geographic covariates on the national scale. The absence of a systematic elevation dependence in the GMST scaling parameter is consistent with previous evidence showing that elevation-dependent warming (EDW) varies substantially among regions and seasons, with no universal elevation–warming relationship at broader spatial scales (Pepin et al., 2022). For example, using high- and low-elevation station networks, Sigro et al. (2024) found negative EDW across mean, maximum, and minimum temperatures in the Sierra Nevada, whereas mean temperature trends in the Pyrenees showed no elevation dependence. In contrast, the scale parameter exhibits pronounced spatial variability across the Iberian Peninsula, with the highest values generally occurring in coastal regions. In Mediterranean coastal regions, variability is strongly influenced by sea surface temperature, land–sea thermal contrasts and marine air advection (Barkhordarian et al., 2025). Differently, Ebro Valley heat extremes are linked to pronounced continentality, complex topography, and channeling and downslope winds (Cebrián et al., 2023). Finally, over the dry central plateau, summer evapotranspiration is often suppressed, making interannual TXx variability around its warming trend less responsive to additional soil drying than in wetter transitional climate regions (Seneviratne et al., 2010). At the same time, limited soil moisture reduces evaporative cooling and can enhance the warming response of TXx to increasing GMST. Thus, low year-to-year variability and enhanced background sensitivity can coexist over the plateau, reflecting two distinct expressions of the same soil-moisture constraint: one dampening short-term fluctuations, the other reinforcing the long-term trend. For autumn Rx1day, both the location and scale parameters exhibit clear relationships with elevation and distance to the sea, with more intense and variable precipitation extremes at higher elevations and near the coast. This pattern is consistent with the combined influence of orographic forcing and moisture availability from the surrounding seas reported for precipitation extremes in Spain (Camarasa-Belmonte and Soriano, 2014; Gonzalez-Hidalgo et al., 2025; Ramis et al., 2013; Serrano-Notivoli et al., 2017). Overall, geographic factors shape the spatial distribution of extreme temperature and precipitation, and this information is useful for modeling them.

https://doi.org/10.5194/egusphere-2026-6347
Preprint. Discussion started: 5 November 2026
© Author(s) 2026. CC BY 4.0 License.

Spatial models also enable prediction of the fitted extreme value distribution at unobserved locations, from which return levels and return periods can be derived consistently, extending the applicability of the model beyond the monitoring network and supporting risk assessment in ungauged regions (Miniussi and Marra, 2021). This prediction capability of the GEVD parameters and return periods at new locations is exploited to obtain grid-based results ensuring complete coverage of peninsular Spain. Although this could be achieved by applying a GEVD to each grid point in an observational database such as E-OBS (Haylock et al., 2008) or the ERA5 reanalysis (Hersbach et al., 2020), time series from irregularly distributed weather stations provide a better representation of extremes than regular grids representing area averages, which tend to smooth local extremes, leading to a systematic underestimation of extremes (Hofstra et al., 2009, 2010; Velikou et al., 2022; Gomis-Cebolla et al., 2023). Therefore, predicting extremes at new locations offers a way to obtain spatially continuous, grid-based estimates for the whole of peninsular Spain while retaining the fidelity to station-level extremes that gridded interpolation products tend to lose. Similar approaches interpolating extreme-value statistics rather than the daily observations themselves have been recommended for spatial mapping of climate extremes in USA (Risser et al., 2019). A comprehensive comparison of the return levels obtained in our regular grid with those obtained by applying EVT directly to gridded datasets in Spain is beyond the scope of this study and should be addressed in future research to quantify the differences and assess the implications of each approach.

Finally, the two inference strategies show a clear trade-off rather than a simple ranking. MCMC yields a faithful characterization of the posterior and its dependence structure, while the Laplace approximation departs from multivariate normality and can misrepresent parameter CIs. Even so, point estimates from both approaches largely agree, so Laplace remains a reasonable choice where speed matters more than a fully accurate uncertainty quantification, for instance in exploratory analyses or when screening many stations before committing to full MCMC fits.

6 Conclusions

This study analyzes daily temperature and precipitation extremes in mainland Spain over the period 1981–2022 and their relationship to climate change, with a particular focus on identifying the most appropriate formulations for modeling these extremes in both space and time, and deriving the associated return levels. A Generalized Extreme Value Distribution (GEVD) was fitted to daily summer TXx and autumn Rx1day extremes, incorporating climate change signals (stationary vs. non-stationary models) and spatial information (spatial vs. local models). Model inference relied on two Bayesian inference methods (Markov Chain Monte Carlo, MCMC vs. Laplace approximation) and spatial interpolation approaches (fully Bayesian spatial model vs. two-step kriging-local approach), providing uncertainty estimates for distribution parameters and return periods. Special emphasis was placed on developing spatial models trained on weather station data that could predict extremes at unobserved locations across the peninsula, thereby extending station-based inference to areas without direct observational coverage. The main conclusions of this study are:

https://doi.org/10.5194/egusphere-2026-6347
Preprint. Discussion started: 5 November 2026
© Author(s) 2026. CC BY 4.0 License.

- Regarding climate change signals, we find contrasting responses across extreme types. For summer TXx, a non-stationary model with location parameters conditioned on Global Mean Surface Temperature (GMST) provided a better fit than its stationary counterpart, indicating an intensification of summer temperature extremes, which are warming faster than GMST. In contrast, autumn Rx1day was better described by a stationary model, suggesting that any climate change influence on autumn precipitation extremes remains undetectable with the available data.
- MCMC provided the most robust characterization of posterior uncertainty, whereas the Laplace approximation, although considerably faster, showed discrepancies in some GEVD parameters. This reflects the fact that the posterior distribution, particularly when spatial and temporal dependencies are incorporated, does not fully satisfy the multivariate normality assumption of the Laplace approximation. Nevertheless, when highly precise GEVD parameter estimates are not required, the Laplace approximation is a reasonable and faster alternative.
- The fully Bayesian spatial model incorporating spatial dependence into the fitting process offered a more coherent quantification of uncertainty and narrower credible intervals than the two-step approach, in which the local GEVD parameters are spatially interpolated by universal kriging. The improvement varied with the extreme type, being particularly valuable for the non-stationary summer TXx model. For the stationary Rx1day model, the two-step approach performed better (except in regions prone to very heavy rainfall), although it tended to underestimate extreme values.
- The spatial models revealed how these extremes depend on geographic and climatic covariates. For summer TXx, the magnitude of extreme temperatures decreased with elevation and with proximity to the sea, whereas interannual variability was greater in coastal regions. The climate change signal showed no significant geographic dependence. Differently, precipitation extremes exhibited a dependence on elevation and distance to the coast, affecting both their mean intensity and variability, with the highest values occurring in coastal and high-elevation regions.

As global warming increases, summer temperature extremes shift toward higher values, leading to an increased likelihood of exceeding present-day extreme thresholds under our fitted non-stationary model. This has direct implications for infrastructure and public health planning, since thresholds currently designed around today's extremes would need to account for a markedly hotter tail of the temperature distribution in the future. Although no significant climate change signal was detected for autumn Rx1day, regions along the Mediterranean coast and northeastern Spain already experience exceptionally severe high-impact rainfall extremes, requiring continued adaptation measures despite the absence of a detectable climate change trend.

Code and data availability

The AEMET observational data used in this study were provided upon request and are subject to the data access conditions of the Spanish State Meteorological Agency (AEMET). The scripts used for the analyses are openly available in a Zenodo repository (DOI: 10.5281/zenodo.23043055).

https://doi.org/10.5194/egusphere-2026-6347
Preprint. Discussion started: 5 November 2026
© Author(s) 2026. CC BY 4.0 License.

Supplement link

The link to the supplement will be included by Copernicus, if applicable.

Author contributions

All authors contributed to the conception and design of the study. Material preparation, data collection, and formal analysis were performed by S.C., D.B., J.A.G., and S.B. Methodology development and software implementation were carried out by S.C., J.A.G., and J.E.J. Supervision was provided by R.G.-H. and S.M.V.-S. The first draft of the manuscript was written by S.C. and all authors commented on previous versions of the manuscript. All authors read and approved the final manuscript.

Competing interests

The authors have no relevant financial or non-financial interests to disclose.

Acknowledgements

This research was supported by the MaX-CSIC Excellence Award. We thank the Spanish State Meteorological Agency (AEMET) and CSIC's Interdisciplinary Thematic Platform Clima (PTI-Clima) for providing and curating the data.

Financial support

This work was supported by the European Commission NextGenerationEU (Regulation EU 2020/2094) through CSIC's Interdisciplinary Thematic Platform Clima (PTI-Clima; Ref. CSC2304000). This research is supported by the MaX-CSIC Excellence Award DEEP-MaX-2024-2_IGEO.

References

Ahmad, T., Ahmad, I., Arshad, I. A., and Bianco, N.: A comprehensive study on the Bayesian modelling of extreme rainfall: A case study from Pakistan, International Journal of Climatology, 42, 208–224, https://doi.org/10.1002/joc.7240, 2022.

Andria, S., Borga, M., and Marani, M.: Thermodynamic Versus Large-Scale Controls on Extreme Precipitation: Temporal Scale Dependence and Clausius-Clapeyron Scaling Redefined, Geophys. Res. Lett., 52, e2025GL115204, https://doi.org/10.1029/2025GL115204, 2025.

Bacro, J.-N., Gaetan, C., Opitz, T., and Toulemonde, G.: Hierarchical Space-Time Modeling of Asymptotically Independent Exceedances With an Application to Precipitation Data, J. Am. Stat. Assoc., 115, 555–569, https://doi.org/10.1080/01621459.2019.1617152, 2020.

https://doi.org/10.5194/egusphere-2026-6347
Preprint. Discussion started: 5 November 2026
© Author(s) 2026. CC BY 4.0 License.

Barkhordarian, A., Brunet, E., and Baehr, J.: Compound coastal marine–terrestrial heatwaves associated with humid-heat stress in Europe, Sci. Rep., 15, 43810, https://doi.org/10.1038/s41598-025-32049-z, 2025.

Barriopedro, D., Jiménez-Esteve, B., Collazo, S., Garrido-Perez, J. M., Johnson, J. E., and García-Herrera, R.: A Multimethod Attribution Analysis of Spain's 2024 Extreme Precipitation Event, Bull. Am. Meteorol. Soc., 106, E2440–E2460, https://doi.org/10.1175/BAMS-D-25-0049.1, 2025.

Beguería, S., Tomas-Burguera, M., Serrano-Notivoli, R., Barriopedro, D., and Vicente-Serrano, S. M.: Evolution of extreme precipitation in Spain: contribution of atmospheric dynamics and long-term trends, Stochastic Environmental Research and Risk Assessment, 39, 2137–2157, https://doi.org/10.1007/s00477-025-02961-x, 2025.

Blanchet, J. and Lehning, M.: Mapping snow depth return levels: smooth spatial modeling versus station interpolation, Hydrol. Earth Syst. Sci., 14, 2527–2544, https://doi.org/10.5194/hess-14-2527-2010, 2010.

Bousquet, N.: Bayesian Extreme Value Theory, in: Extreme Value Theory with Applications to Natural Hazards, Springer International Publishing, Cham, 271–325, https://doi.org/10.1007/978-3-030-74942-2_11, 2021.

Brooks, S., Gelman, A., Jones, G., and Meng, X.-L.: Handbook of Markov Chain Monte Carlo, Chapman and Hall/CRC, New York, https://doi.org/10.1201/b10905, 2011.

C3S/ECMWF and WMO: C3S-WMO European State of the Climate 2025, https://doi.org/10.24381/zy93-sb27, 2026.

Calvo-Sancho, C., Díaz-Fernández, J., González-Alemán, J. J., Halifa-Marín, A., Miglietta, M. M., Azorin-Molina, C., Prein, A. F., Montoro-Mendoza, A., Bolgiani, P., Morata, A., and Martín, M. L.: Human-induced climate change amplification on storm dynamics in Valencia's 2024 catastrophic flash flood, Nat. Commun., 17, 1492, https://doi.org/10.1038/s41467-026-68929-9, 2026.

Camarasa-Belmonte, A. M. and Soriano, J.: Empirical study of extreme rainfall intensity in a semi-arid environment at different time scales, J. Arid Environ., 100–101, 63–71, https://doi.org/10.1016/j.jaridenv.2013.10.008, 2014.

Carney, M. C.: Bias Correction to GEV Shape Parameters Used to Predict Precipitation Extremes, J. Hydrol. Eng., 21, 04016035, https://doi.org/10.1061/(ASCE)HE.1943-5584.0001416, 2016.

Carpenter, B., Gelman, A., Hoffman, M. D., Lee, D., Goodrich, B., Betancourt, M., Brubaker, M., Guo, J., Li, P., and Riddell, A.: Stan: A Probabilistic Programming Language, J. Stat. Softw., 76, 1–32, https://doi.org/10.18637/jss.v076.i01, 2017.

Castillo-Mateo, J., Cebrián, A. C., and Asín, J.: Statistical analysis of extreme and record-breaking daily maximum temperatures in peninsular Spain during 1960–2021, Atmos. Res., 293, 106934, https://doi.org/10.1016/j.atmosres.2023.106934, 2023.

Castro-Camilo, D. and Huser, R.: Local Likelihood Estimation of Complex Tail Dependence Structures, Applied to U.S. Precipitation Extremes, J. Am. Stat. Assoc., 115, 1037–1054, https://doi.org/10.1080/01621459.2019.1647842, 2020.

Cebrián, A. C., Asín, J., Castillo-Mateo, J., Gelfand, A. E., and Abaurrea, J.: Assessing space and time changes in daily maximum temperature in the Ebro basin (Spain) using model-based statistical tools, International Journal of Climatology, 43, 8036–8051, https://doi.org/10.1002/joc.8305, 2023.

https://doi.org/10.5194/egusphere-2026-6347
Preprint. Discussion started: 5 November 2026
© Author(s) 2026. CC BY 4.0 License.

Chazarra Bernabé, A., Flórez García, E., Peraza Sánchez, B., Tohá Rebull, T., Lorenzo Mariño, B., Criado Pinto, E., Moreno García, J. V., Romero Fresneda, R., and Botey Fullat, R.: Mapas climáticos de España (1981-2010) y ETo (1996-2016), Agencia Estatal de Meteorología, https://doi.org/10.31978/014-18-004-2, 2018.

Cleveland, W. S., Grosse, E., and Shyu, W. M.: Local regression models, in: Statistical Models in S, edited by: Chambers, J. and Hastie, T., Wadsworth & Brooks/Cole, https://doi.org/10.1201/9780203738535, 1992.

Coles, S.: An Introduction to Statistical Modeling of Extreme Values, Springer London, London, https://doi.org/10.1007/978-1-4471-3675-0, 2001.

Collazo, S., Barriopedro, D., García-Herrera, R., and Beguería, S.: Extreme heat and mortality in the state of Rio de Janeiro in November 2023: attribution to climate change and ENSO, Nat. Hazards Earth Syst. Sci., 25, 3221–3238, https://doi.org/10.5194/nhess-25-3221-2025, 2025.

Cooley, D., Nychka, D., and Naveau, P.: Bayesian Spatial Modeling of Extreme Precipitation Return Levels, J. Am. Stat. Assoc., 102, 824–840, https://doi.org/10.1198/016214506000000780, 2007.

Corell, D., Estrela, M. J., Miró, J. J., Orgambides-García, D., and Niclós, R.: Observed Changes in Maximum and Minimum Temperatures and Daily Temperature Range in the Iberian Peninsula and Balearic Islands Between 1952 and 2022, International Journal of Climatology, 46, e70182, https://doi.org/10.1002/joc.70182, 2026.

Davison, A. C., Padoan, S. A., and Ribatet, M.: Statistical Modeling of Spatial Extremes, Statistical Science, 27, 161–186, https://doi.org/10.1214/11-STS376, 2012.

Diriba, T. A. and Debusho, L. K.: Modelling dependency effect to extreme value distributions with application to extreme wind speed at Port Elizabeth, South Africa: a frequentist and Bayesian approaches, Comput. Stat., 35, 1449–1479, https://doi.org/10.1007/s00180-019-00947-2, 2020.

Durante, D., Pozza, F., and Szabo, B.: Skewed Bernstein–von Mises theorem and skew-modal approximations, The Annals of Statistics, 52, 2714–2737, https://doi.org/10.1214/24-AOS2429, 2024.

Ellison, A. M.: Bayesian inference in ecology, Ecol. Lett., 7, 509–520, https://doi.org/10.1111/j.1461-0248.2004.00603.x, 2004.

Etz, A. and Vandekerckhove, J.: Introduction to Bayesian Inference for Psychology, Psychon. Bull. Rev., 25, 5–34, https://doi.org/10.3758/s13423-017-1262-3, 2018.

Ferreira, R. N.: Cut-Off Lows and Extreme Precipitation in Eastern Spain: Current and Future Climate, Atmosphere, 12, 835, https://doi.org/10.3390/atmos12070835, 2021.

Gabry, J., Simpson, D., Vehtari, A., Betancourt, M., and Gelman, A.: Visualization in Bayesian workflow, J. R. Stat. Soc. A, 182, 389–402, https://doi.org/10.1111/rssa.12378, 2019.

Gabry, J., Češnovar, R., Johnson, A., and Bronder, S.: cmdstanr: R Interface to "CmdStan," https://mc-stan.org/cmdstanr/, 2025.

García, J. A., Martín, J., Naranjo, L., and Acero, F. J.: A Bayesian hierarchical spatio-temporal model for extreme rainfall in Extremadura (Spain), Hydrological Sciences Journal, 63, 878–894, https://doi.org/10.1080/02626667.2018.1457219, 2018.

https://doi.org/10.5194/egusphere-2026-6347
Preprint. Discussion started: 5 November 2026
© Author(s) 2026. CC BY 4.0 License.

García, J. A., Pizarro, M. M., Acero, F. J., and Parra, M. I.: A Bayesian hierarchical spatial copula model: An application to extreme temperatures in Extremadura (Spain), Atmosphere, 12, 897, https://doi.org/10.3390/atmos12070897, 2021.

García, J. A., Acero, F. J., and Portero, J.: A Bayesian hierarchical spatio-temporal model for extreme temperatures in Extremadura (Spain) simulated by a Regional Climate Model, Clim. Dyn., 61, 1489–1503, https://doi.org/10.1007/s00382-022-06638-x, 2023.

García, J. A., Acero, F. J., Martínez-Pizarro, M., and Lara, M.: A Bayesian hierarchical spatio-temporal model for summer extreme temperatures in Spain, Stochastic Environmental Research and Risk Assessment, 38, 3393–3410, https://doi.org/10.1007/s00477-024-02754-8, 2024.

Gelman, A., Jakulin, A., Pittau, M. G., and Su, Y.-S.: A weakly informative default prior distribution for logistic and other regression models, Ann. Appl. Stat., 2, 1360–1383, https://doi.org/10.1214/08-AOAS191, 2008.

Gelman, A., Carlin, J. B., Stern, H. S., Dunson, D. B., Vehtari, A., and Rubin, D. B.: Bayesian Data Analysis, 3rd edn., Chapman and Hall/CRC, Boca Raton, FL, https://doi.org/10.1201/b16018, 2013.

Gelman, A., Hwang, J., and Vehtari, A.: Understanding predictive information criteria for Bayesian models, Stat. Comput., 24, 997–1016, https://doi.org/10.1007/s11222-013-9416-2, 2014.

Goda, Y.: Inherent Negative Bias of Quantile Estimates of Annual Maximum Data Due to Sample Size Effect: A Numerical Simulation Study, Coastal Engineering Journal, 53, 397–429, https://doi.org/10.1142/S0578563411002409, 2011.

Gomis-Cebolla, J., Rattayova, V., Salazar-Galán, S., and Francés, F.: Evaluation of ERA5 and ERA5-Land reanalysis precipitation datasets over Spain (1951–2020), Atmos. Res., 284, 106606, https://doi.org/10.1016/j.atmosres.2023.106606, 2023.

Gonzalez-Hidalgo, J. C., Beguería, S., Peña-Angulo, D., and Blanco, V. T.: Catalogue and Analysis of Extraordinary Precipitation Events in the Spanish Mainland, 1916–2022, International Journal of Climatology, 45, e8785, https://doi.org/10.1002/joc.8785, 2025.

Haylock, M. R., Hofstra, N., Klein Tank, A. M. G., Klok, E. J., Jones, P. D., and New, M.: A European daily high-resolution gridded data set of surface temperature and precipitation for 1950–2006, Journal of Geophysical Research: Atmospheres, 113, D20119, https://doi.org/10.1029/2008JD010201, 2008.

Hersbach, H., Bell, B., Berrisford, P., Hirahara, S., Horányi, A., Muñoz-Sabater, J., Nicolas, J., Peubey, C., Radu, R., Schepers, D., Simmons, A., Soci, C., Abdalla, S., Abellan, X., Balsamo, G., Bechtold, P., Biavati, G., Bidlot, J., Bonavita, M., De Chiara, G., Dahlgren, P., Dee, D., Diamantakis, M., Dragani, R., Flemming, J., Forbes, R., Fuentes, M., Geer, A., Haimberger, L., Healy, S., Hogan, R. J., Hólm, E., Janisková, M., Keeley, S., Laloyaux, P., Lopez, P., Lupu, C., Radnoti, G., de Rosnay, P., Rozum, I., Vamborg, F., Villaume, S., and Thépaut, J.-N.: The ERA5 global reanalysis, Quarterly Journal of the Royal Meteorological Society, 146, 1999–2049, https://doi.org/10.1002/qj.3803, 2020.

Hoffman, M. D. and Gelman, A.: The No-U-Turn Sampler: Adaptively Setting Path Lengths in Hamiltonian Monte Carlo, Journal of Machine Learning Research, 15, 1593–1623, https://jmlr.org/papers/v15/hoffman14a.html, 2014.

https://doi.org/10.5194/egusphere-2026-6347
Preprint. Discussion started: 5 November 2026
© Author(s) 2026. CC BY 4.0 License.

Hofstra, N., Haylock, M., New, M., and Jones, P. D.: Testing E-OBS European high-resolution gridded data set of daily precipitation and surface temperature, Journal of Geophysical Research: Atmospheres, 114, D21101, https://doi.org/10.1029/2009JD011799, 2009.

Hofstra, N., New, M., and McSweeney, C.: The influence of interpolation and station network density on the distributions and trends of climate variables in gridded daily data, Clim. Dyn., 35, 841–858, https://doi.org/10.1007/s00382-009-0698-1, 2010.

Huser, R. and Wadsworth, J. L.: Advances in statistical modeling of spatial extremes, WIREs Computational Statistics, 14, e1537, https://doi.org/10.1002/wics.1537, 2022.

IPCC AR6: Weather and Climate Extreme Events in a Changing Climate, in: Climate Change 2021 – The Physical Science Basis, Cambridge University Press, 1513–1766, https://doi.org/10.1017/9781009157896.013, 2023.

Joshi, M. M., Gregory, J. M., Webb, M. J., Sexton, D. M. H., and Johns, T. C.: Mechanisms for the land/sea warming contrast exhibited by simulations of climate change, Clim. Dyn., 30, 455–465, https://doi.org/10.1007/s00382-007-0306-1, 2008.

Karagiannis, G. P.: Introduction to Bayesian Statistical Inference, in: Uncertainty in Engineering, edited by: Aslett, L. J. M., Coolen, F. P. A., and De Bock, J., SpringerBriefs in Statistics, Springer, Cham, 1–13, https://doi.org/10.1007/978-3-030-83640-5_1, 2022.

Kharin, V. V. and Zwiers, F. W.: Estimating Extremes in Transient Climate Change Simulations, J. Clim., 18, 1156–1173, https://doi.org/10.1175/JCLI3320.1, 2005.

Lambert, B. and Vehtari, A.: R∗: A Robust MCMC Convergence Diagnostic with Uncertainty Using Decision Tree Classifiers, Bayesian Anal., 17, 353–379, https://doi.org/10.1214/20-BA1252, 2022.

Lele, S. R., Glen, C. G., and Ponciano, J. M.: Practical Consequences of the Bias in the Laplace Approximation to Marginal Likelihood for Hierarchical Models, Entropy, 27, 289, https://doi.org/10.3390/e27030289, 2025.

Mardia, K. V.: Tests of univariate and multivariate normality, in: Handbook of Statistics, Vol. 1, Analysis of Variance, edited by: Krishnaiah, P. R., Elsevier, Amsterdam, 279–320, https://doi.org/10.1016/S0169-7161(80)01011-5, 1980.

Martins, E. S. and Stedinger, J. R.: Generalized maximum-likelihood generalized extreme-value quantile estimators for hydrologic data, Water Resour. Res., 36, 737–744, https://doi.org/10.1029/1999WR900330, 2000.

Matheron, G.: Universal kriging, in: Matheron's Theory of Regionalised Variables, edited by: Pawlowsky-Glahn, V. and Serra, J., Oxford University Press, 123–180, https://doi.org/10.1093/oso/9780198835660.003.0005, 2019.

Met Office: HadCRUT5 global annual mean temperature anomalies [data set], https://www.metoffice.gov.uk/hadobs/hadcrut5/, 2024.

Miniussi, A. and Marra, F.: Estimation of extreme daily precipitation return levels at-site and in ungauged locations using the simplified MEV approach, J. Hydrol., 603, 126946, https://doi.org/10.1016/j.jhydrol.2021.126946, 2021.

Morice, C. P., Kennedy, J. J., Rayner, N. A., Winn, J. P., Hogan, E., Killick, R. E., Dunn, R. J. H., Osborn, T. J., Jones, P. D., and Simpson, I. R.: An Updated Assessment of Near-Surface Temperature Change From 1850: The HadCRUT5 Data Set, J. Geophys. Res. Atmos., 126, e2019JD032361, https://doi.org/10.1029/2019JD032361, 2021.

https://doi.org/10.5194/egusphere-2026-6347
Preprint. Discussion started: 5 November 2026
© Author(s) 2026. CC BY 4.0 License.

Neal, R. M.: MCMC Using Hamiltonian Dynamics, in: Handbook of Markov Chain Monte Carlo, Chapman and Hall/CRC, New York, 113–162, https://doi.org/10.1201/b10905-6, 2011.

Nguyen, A. B. H., Bonici, M., McGee, G., and Percival, W. J.: LOO-PIT: A sensitive posterior test, Journal of Cosmology and Astroparticle Physics, 2025, 008, https://doi.org/10.1088/1475-7516/2025/01/008, 2025.

O'Gorman, P. A.: Precipitation Extremes Under Climate Change, Curr. Clim. Change Rep., 1, 49–59, https://doi.org/10.1007/s40641-015-0009-3, 2015.

Pepin, N. C., Arnone, E., Gobiet, A., Haslinger, K., Kotlarski, S., Notarnicola, C., Palazzi, E., Seibert, P., Serafin, S., Schöner, W., Terzago, S., Thornton, J. M., Vuille, M., and Adler, C.: Climate Changes and Their Elevational Patterns in the Mountains of the World, Reviews of Geophysics, 60, e2020RG000730, https://doi.org/10.1029/2020RG000730, 2022.

Philip, S., Kew, S., van Oldenborgh, G. J., Otto, F., Vautard, R., van der Wiel, K., King, A., Lott, F., Arrighi, J., Singh, R., and van Aalst, M.: A protocol for probabilistic extreme event attribution analyses, Adv. Stat. Climatol. Meteorol. Oceanogr., 6, 177–203, https://doi.org/10.5194/ascmo-6-177-2020, 2020.

PTI-Clima: PTI-Clima project, Consejo Superior de Investigaciones Científicas, https://pti-clima.csic.es/, last access: 22 July 2026, 2026.

Ramis, C., Homar, V., Amengual, A., Romero, R., and Alonso, S.: Daily precipitation records over mainland Spain and the Balearic Islands, Natural Hazards and Earth System Sciences, 13, 2483–2491, https://doi.org/10.5194/nhess-13-2483-2013, 2013.

Renard, B.: A Bayesian hierarchical approach to regional frequency analysis, Water Resour. Res., 47, W11513, https://doi.org/10.1029/2010WR010089, 2011.

Risser, M. D., Paciorek, C. J., Wehner, M. F., O'Brien, T. A., and Collins, W. D.: A probabilistic gridded product for daily precipitation extremes over the United States, Clim. Dyn., 53, 2517–2538, https://doi.org/10.1007/s00382-019-04636-0, 2019.

Robin, Y. and Ribes, A.: Nonstationary extreme value analysis for event attribution combining climate models and observations, Adv. Stat. Climatol. Meteorol. Oceanogr., 6, 205–221, https://doi.org/10.5194/ascmo-6-205-2020, 2020.

Roksvåg, T., Lutz, J., Grinde, L., Dyrrdal, A. V., and Thorarinsdottir, T. L.: Consistent intensity-duration-frequency curves by post-processing of estimated Bayesian posterior quantiles, J. Hydrol., 603, 127000, https://doi.org/10.1016/j.jhydrol.2021.127000, 2021.

Rue, H. and Martino, S.: Approximate Bayesian inference for hierarchical Gaussian Markov random field models, J. Stat. Plan. Inference, 137, 3177–3192, https://doi.org/10.1016/j.jspi.2006.07.016, 2007.

Rue, H., Martino, S., and Chopin, N.: Approximate Bayesian Inference for Latent Gaussian models by using Integrated Nested Laplace Approximations, J. R. Stat. Soc. Series B Stat. Methodol., 71, 319–392, https://doi.org/10.1111/j.1467-9868.2008.00700.x, 2009.

Sang, H. and Gelfand, A. E.: Continuous Spatial Process Models for Spatial Extreme Values, J. Agric. Biol. Environ. Stat., 15, 49–65, https://doi.org/10.1007/s13253-009-0010-1, 2010.

https://doi.org/10.5194/egusphere-2026-6347
Preprint. Discussion started: 5 November 2026
© Author(s) 2026. CC BY 4.0 License.

Seneviratne, S. I., Corti, T., Davin, E. L., Hirschi, M., Jaeger, E. B., Lehner, I., Orlowsky, B., and Teuling, A. J.: Investigating soil moisture-climate interactions in a changing climate: A review, Earth-Sci. Rev., 99, 125–161, https://doi.org/10.1016/j.earscirev.2010.02.004, 2010.

Serrano-Notivoli, R., Beguería, S., Saz, M. Á., Longares, L. A., and de Luis, M.: SPREAD: a high-resolution daily gridded precipitation dataset for Spain – an extreme events frequency and intensity overview, Earth Syst. Sci. Data, 9, 721–738, https://doi.org/10.5194/essd-9-721-2017, 2017.

Serrano-Notivoli, R., Lemus-Canovas, M., Barrao, S., Sarricolea, P., Meseguer-Ruiz, O., and Tejedor, E.: Heat and cold waves in mainland Spain: Origins, characteristics, and trends, Weather Clim. Extrem., 37, 100471, https://doi.org/10.1016/j.wace.2022.100471, 2022.

Sigro, J., Cisneros, M., Perez-Luque, A. J., Perez-Martinez, C., and Vegas-Vilarrubia, T.: Trends in temperature and precipitation at high and low elevations in the main mountain ranges of the Iberian Peninsula (1894–2020): The Sierra Nevada and the Pyrenees, International Journal of Climatology, 44, 2897–2920, https://doi.org/10.1002/joc.8487, 2024.

Stan Development Team: Stan User's Guide, https://mc-stan.org/docs/stan-users-guide/, last access: July 2026, 2025.

Stott, P. A., Christidis, N., Otto, F. E. L., Sun, Y., Vanderlinden, J., van Oldenborgh, G. J., Vautard, R., von Storch, H., Walton, P., Yiou, P., and Zwiers, F. W.: Attribution of extreme weather and climate-related events, WIREs Climate Change, 7, 23–41, https://doi.org/10.1002/wcc.380, 2016.

Stringer, A., Brown, P., and Stafford, J.: Fast, Scalable Approximations to Posterior Distributions in Extended Latent Gaussian Models, Journal of Computational and Graphical Statistics, 32, 84–98, https://doi.org/10.1080/10618600.2022.2099403, 2023.

Szolgay, J., Parajka, J., Kohnová, S., and Hlavčová, K.: Comparison of mapping approaches of design annual maximum daily precipitation, Atmos. Res., 92, 289–307, https://doi.org/10.1016/j.atmosres.2009.01.009, 2009.

UNEP: Emissions Gap Report 2025: Off Target - Continued Collective inaction puts Global Temperature Goal at Risk, United Nations Environment Programme, https://doi.org/10.59117/20.500.11822/48854, 2025.

Urrea Méndez, D. and del Jesus, M.: Estimating extreme monthly rainfall for Spain using non-stationary techniques, Hydrological Sciences Journal, 68, 903–919, https://doi.org/10.1080/02626667.2023.2193294, 2023.

Vautard, R., Cattiaux, J., Happé, T., Singh, J., Bonnet, R., Cassou, C., Coumou, D., D'Andrea, F., Faranda, D., Fischer, E., Ribes, A., Sippel, S., and Yiou, P.: Heat extremes in Western Europe increasing faster than simulated due to atmospheric circulation trends, Nat. Commun., 14, 6803, https://doi.org/10.1038/s41467-023-42143-3, 2023.

Vehtari, A., Gelman, A., and Gabry, J.: Practical Bayesian model evaluation using leave-one-out cross-validation and WAIC, Stat. Comput., 27, 1413–1432, https://doi.org/10.1007/s11222-016-9696-4, 2017.

Velikou, K., Lazoglou, G., Tolika, K., and Anagnostopoulou, C.: Reliability of the ERA5 in Replicating Mean and Extreme Temperatures across Europe, Water, 14, 543, https://doi.org/10.3390/w14040543, 2022.

Vicente-Serrano, S. M., Rodríguez-Camino, E., Domínguez-Castro, F., El Kenawy, A., and Azorín-Molina, C.: An updated review on recent trends in observational surface atmospheric variables and their extremes over Spain, Cuadernos de Investigación Geográfica, 43, 209–232, https://doi.org/10.18172/cig.3134, 2017.

https://doi.org/10.5194/egusphere-2026-6347
Preprint. Discussion started: 5 November 2026
© Author(s) 2026. CC BY 4.0 License.

Vicente-Serrano, S. M., Tramblay, Y., Reig, F., González-Hidalgo, J. C., Beguería, S., Brunetti, M., Kalin, K. C., Patalen, L., Kržič, A., Lionello, P., Lima, M. M., Trigo, R. M., El-Kenawy, A. M., Eddenjal, A., Türkes, M., Koutroulis, A., Manara, V., Maugeri, M., Badi, W., Mathbout, S., Bertalanič, R., Bocheva, L., Dabanli, I., Dumitrescu, A., Dubuisson, B., Sahabi-Abed, S., Abdulla, F., Fayad, A., Hodzic, S., Ivanov, M., Radevski, I., Peña-Angulo, D., Lorenzo-Lacruz, J., Domínguez-Castro, F., Gimeno-Sotelo, L., García-Herrera, R., Franquesa, M., Halifa-Marín, A., Adell-Michavila, M., Noguera, I., Barriopedro, D., Garrido-Perez, J. M., Azorin-Molina, C., Andres-Martin, M., Gimeno, L., Nieto, R., Llasat, M. C., Markonis, Y., Selmi, R., Ben Rached, S., Radovanović, S., Soubeyroux, J.-M., Ribes, A., Saidi, M. E., Bataineh, S., El Khalki, E. M., Robaa, S., Boucetta, A., Alsafadi, K., Mamassis, N., Mohammed, S., Fernández-Duque, B., Cheval, S., Moutia, S., Stevkov, A., Stevkova, S., Luna, M. Y., and Potopová, V.: High temporal variability not trend dominates Mediterranean precipitation, Nature, 639, 658–666, https://doi.org/10.1038/s41586-024-08576-6, 2025a.

Vicente-Serrano, S. M., Garrido-Perez, J. M., Fernández-Álvarez, J. C., Gimeno-Sotelo, L., Beguería, S., Halifa-Marín, A., Latorre, B., El Kenawy, A. M., Franquesa, M., Adell-Michavila, M., Domínguez-Castro, F., Barriopedro, D., Gimeno-Presa, L., Nieto, R., Azorin-Molina, C., Andres-Martin, M., Gutiérrez, J. M., and García-Herrera, R.: Characteristics of widespread extreme precipitation events in Peninsular Spain and the Balearic Islands: spatio-temporal dynamics and driving mechanisms, Clim. Dyn., 63, 340, https://doi.org/10.1007/s00382-025-07829-y, 2025b.

Watanabe, S.: Asymptotic Equivalence of Bayes Cross Validation and Widely Applicable Information Criterion in Singular Learning Theory, Journal of Machine Learning Research, 11, 3571–3594, https://jmlr.org/papers/v11/watanabe10a.html, 2010.

Yılmaz, A., Kara, M., and Özdemir, O.: Comparison of different estimation methods for extreme value distribution, J. Appl. Stat., 48, 2259–2284, https://doi.org/10.1080/02664763.2021.1940109, 2021.

Zanger, L., Bücher, A., Kreienkamp, F., Lorenz, P., and Tradowsky, J. S.: Regional pooling in extreme event attribution studies: an approach based on multiple statistical testing, Extremes, 27, 1–32, https://doi.org/10.1007/s10687-023-00480-y, 2024.

Zhang, L., Risser, M. D., Molter, E. M., Wehner, M. F., and O'Brien, T. A.: Accounting for the spatial structure of weather systems in detected changes in precipitation extremes, Weather Clim. Extrem., 38, 100499, https://doi.org/10.1016/j.wace.2022.100499, 2022.

Zitzmann, S. and Hecht, M.: Going Beyond Convergence in Bayesian Estimation: Why Precision Matters Too and How to Assess It, Struct. Equ. Modeling, 26, 646–661, https://doi.org/10.1080/10705511.2018.1545232, 2019.